

FULL PAPER

Open Access



Simulation of great earthquakes along the Nankai Trough: reproduction of event history, slip areas of the Showa Tonankai and Nankai earthquakes, heterogeneous slip-deficit rates, and long-term slow slip events

Fuyuki Hirose^{1*} , Kenji Maeda¹ , Kenichi Fujita² and Akio Kobayashi¹ 

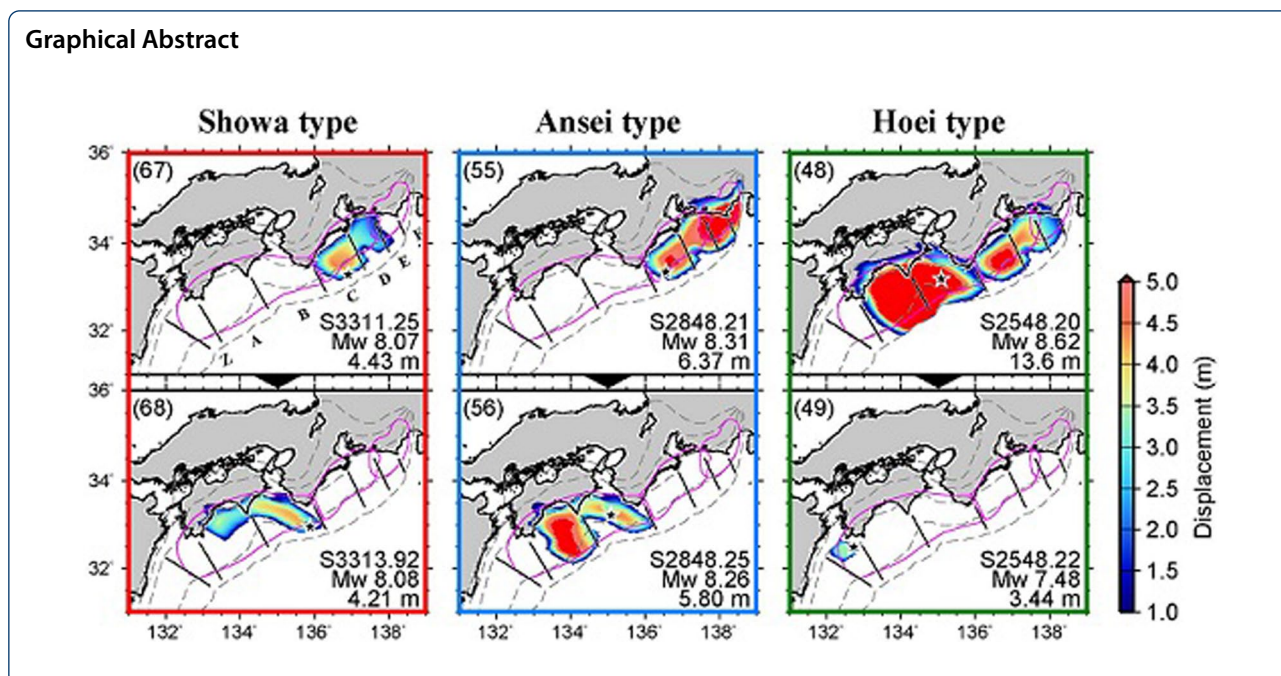
Abstract

Great earthquakes have occurred repeatedly along the Nankai Trough, but only for recent events are details known, such as rupture areas and time lags between paired events. It is meaningful for disaster prevention to consider in advance what kind of phenomena are likely after an earthquake that partially ruptures a seismogenic zone in this region. We constructed three-dimensional simulations to partially reproduce the spatial and temporal distribution of seismic or aseismic slip and the heterogeneous distribution of the slip-deficit rate beneath the seafloor on the plate boundary along the Nankai Trough. We found it necessary to assign spatial heterogeneity to two friction parameters, the effective normal stress and characteristic distance, based on a hierarchical asperity model. Our model produced many event pairs consisting of events east and west of Cape Shiono (Tokai/Tonankai and Nankai events, respectively), nearly all of them either simultaneous or separated by less than 3 years. The rupture areas of these event pairs were rich in variation, and even when the rupture areas were the same, the magnitudes and maximum displacements differed. The Tonankai earthquakes rarely occurred alone. Our model also simulated recurring long-term slow slip events in deeper parts of the seismogenic zone, and these events were caused by stress disturbance and heterogeneous stress distributions associated with non-ruptured portions of the seismogenic zone.

Keywords: Nankai Trough, Numerical simulation, Slip-deficit rate, Long-term slow slip events

*Correspondence: fhirose@mri-jma.go.jp

¹ Meteorological Research Institute, Japan Meteorological Agency, 1-1 Nagamine, Tsukuba, Ibaraki 305-0052, Japan
Full list of author information is available at the end of the article



Introduction

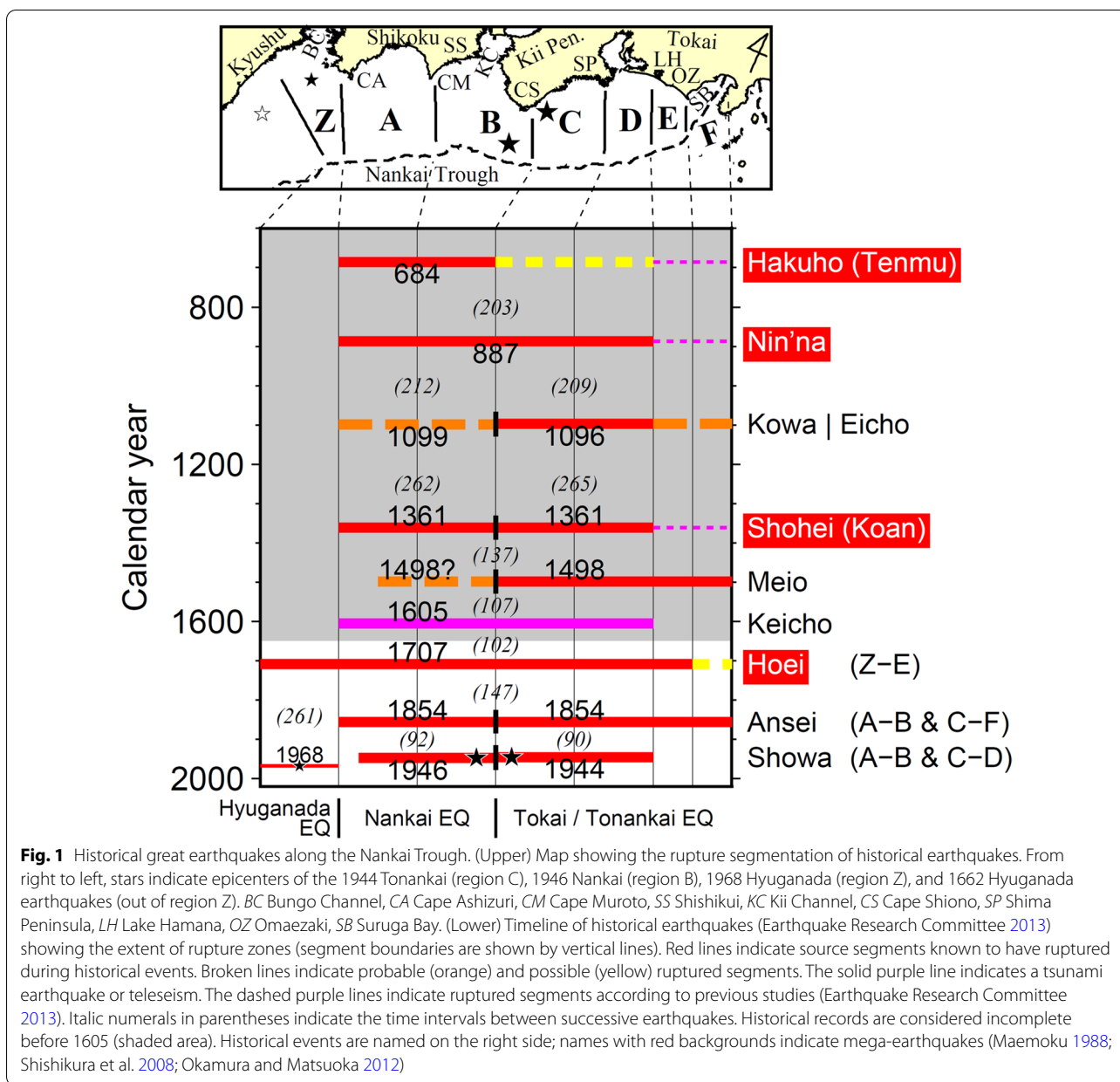
In the Nankai Trough subduction zone off southwestern Japan, where the Philippine Sea plate subducts north-westward beneath the Amur continental plate, many great earthquakes, with moment magnitude (M_w) ~ 8 or larger, are attested in human records (Earthquake Research Committee 2013). These large events have followed one of two patterns: Either the eastern (Tokai/Tonankai) and western (Nankai) segments rupture simultaneously, or these two segments rupture sequentially after a time interval of up to about 3 years (Fig. 1; Table 1). However, the rupture areas of these earthquake pairs differ in detail (Figs. 1, 2). More than 70 years have now passed since the last Nankai earthquake in 1946, and another great Nankai earthquake may be imminent. The recurrence interval of $M_w \sim 8.5$ events (referred to here as mega-earthquakes) such as the 1707 Hoei earthquake (Fig. 2c) has been estimated at 400–600 years (Maemoku 1988; Shishikura et al. 2008; Okamura and Matsuoka 2012). The asperity in the northern part of the Hyuganada sector, adjacent to the Nankai sector, was ruptured in 1707 and 1968, for a recurrence interval of about 260 years (Fig. 1). The plate boundary along the Nankai Trough has several local maxima in slip-deficit rates, and regions with relatively low slip-deficit rates have been identified off the Shima Peninsula, off Cape Shiono, southeast of Cape Muroto, and off Cape Ashizuri (Fig. 2d) (Yokota et al. 2016; Nishimura et al. 2018).

Slow earthquakes including short-term slow slip events (SSSEs) and long-term slow slip events (LSSEs) occur

at the shallow and deep edges of the seismogenic zone (Obara and Kato 2016). LSSEs of moderate size (M_w 6–7) have occurred repeatedly at depths of 20–30 km (e.g., Kobayashi 2014, 2017; Ozawa 2017), near the deep edge of the seismogenic zone (Figs. 2b, 3). In Mexico, an M_w 7-class earthquake occurred on the shallow plate boundary about 2 months after an LSSE on the deep plate boundary beneath Guerrero (Radiguet et al. 2016), and the possibility that deep-seated LSSEs similarly influence great earthquakes along the Nankai Trough is a matter of concern. Because the Hyuganada asperity, capable of M_w 7.5-class earthquakes (Yagi et al. 1998), is also adjacent to the source areas of great earthquakes along the Nankai Trough, it is important to evaluate its influence on Nankai Trough events (e.g., Hyodo et al. 2016).

Simulations of the earthquake cycle based on the rate- and state-dependent friction (RSF) law have been conducted to investigate the occurrence patterns of great earthquakes along the Nankai Trough (e.g., Hori 2006; Hyodo and Hori 2013; Hirose and Maeda 2013; Nakata et al. 2014; Hyodo et al. 2016). However, all of these have focused only on particular phenomena; thus, a comprehensive investigation of seismic phenomena along the Nankai Trough is still needed.

In summary, our purpose was to construct a three-dimensional (3-D) numerical model based on the RSF law to simulate comprehensively, and clarify the characteristics of the parameters that affect, the following phenomena on the Nankai Trough plate boundary:



1. The diversity of the occurrence pattern of great earthquakes
 - 1a The along-strike extent of rupture areas.
 - 1b The recurrence intervals of the three most recent historical event pairs.
 - 1c The time lags between Tokai/Tonankai and Nankai earthquakes.
 - 1d The recurrence interval of mega-earthquakes such as the 1707 Hоеi earthquake.
- 1e The relatively well-determined epicenters and slip distributions of the 1944 Tonankai and 1946 Nankai earthquakes.
2. The occurrence interval of events in the northern Hyuganada sector.
3. The heterogeneous distribution of slip-deficit rates.
4. The recurring LSSEs in the Tokai district, the Kii Channel, western Shikoku, and the Bungo Channel.

Table 1 Occurrence times and magnitudes (M_u , Utsu magnitude; M_t , tsunami magnitude) of historical great earthquakes along the Nankai Trough (Earthquake Research Committee 2013) and our target magnitude range (M_{target}) for each of those earthquakes

Name	Occurrence Time	Magnitude		
		M_u	M_t	M_{target}
Shohei (Koan) Tokai	Aug. 1 or 3, 1361	–	–	–
Shohei (Koan) Nankai	Aug. 3, 1361	8.3–8.5	–	–
Meio Tokai	Sep. 20, 1498	8.2–8.4	8.5	–
Keicho	Feb. 3, 1605	7.9	8.2	–
Hoei	Oct. 28, 1707	8.6	8.4	8.4–8.6
Ansei Tokai	Dec. 23, 1854	8.4	8.3	8.3–8.4
Ansei Nankai	Dec. 24, 1854	8.4	8.3	8.3–8.4
Showa Tonankai	Dec. 7, 1944	7.9	8.1	7.9–8.1
Showa Nankai	Dec. 21, 1946	8.0	8.1	8.0–8.1

This study is based on the standard quasi-dynamic simulation framework (see Sect. 3) that has been used for many years in simulations of the Nankai Trough plate boundary (e.g., Hori 2006; Hyodo and Hori 2013; Hirose and Maeda 2013; Nakata et al. 2014; Hyodo et al. 2016). We hope this study will serve as a guide for those constructing future models in the same framework.

Targeted phenomena

Although the rupture areas of these great earthquake pairs (target phenomenon 1a) are generally similar, they differ in detail (Figs. 1, 2). For example, during the three most recent event pairs (the 1707 Hoei, 1854 Ansei, and 1944/1946 Showa events), the eastern edge of the rupture (eastern segment) was at Cape Omaezaki (1707), Suruga Bay (1854), and Lake Hamana (1944), respectively (Matsu'ura 2012; Earthquake Research Committee 2013). The eastern edge of the 1707 Hoei earthquake rupture,

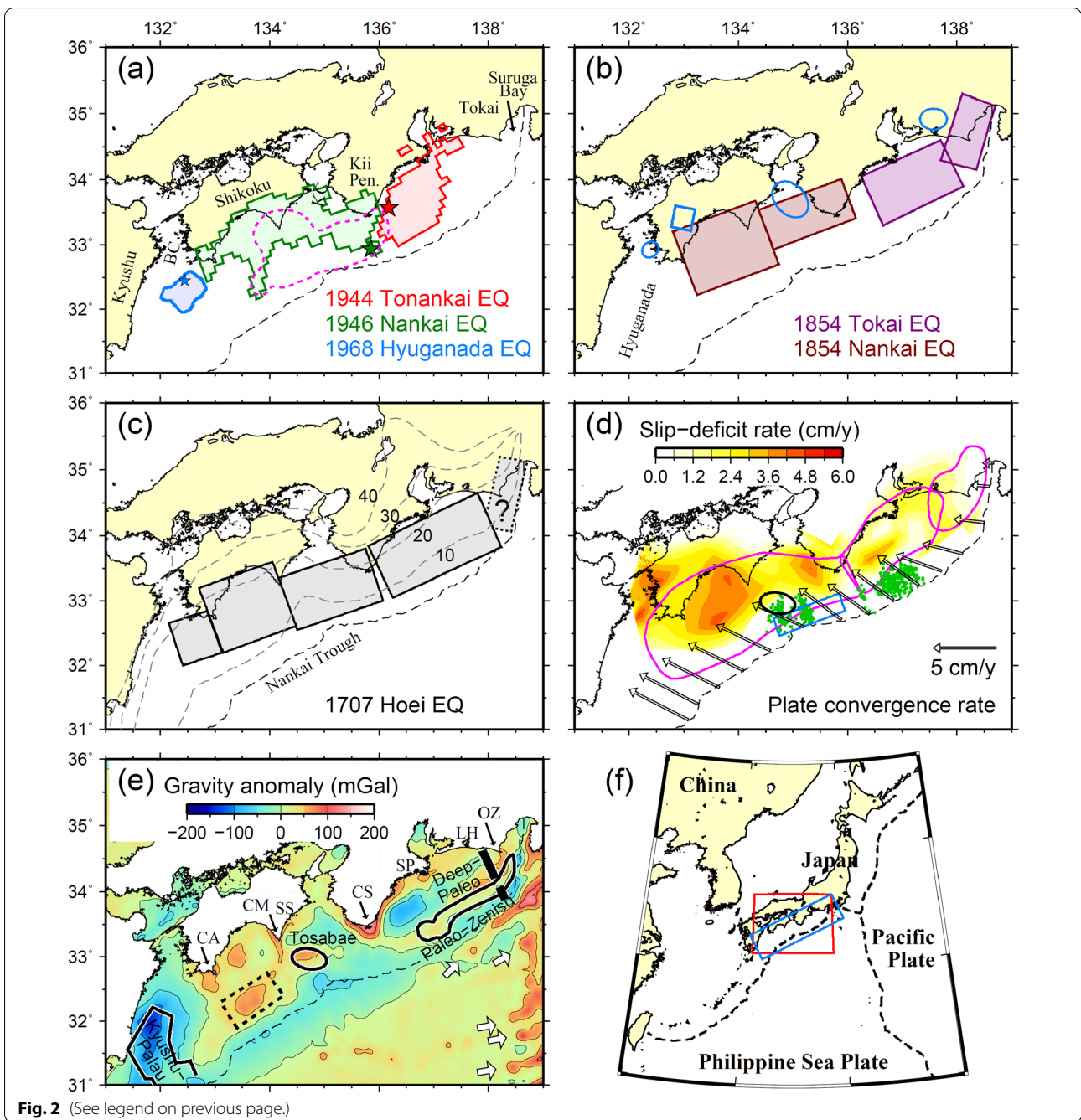
previously considered to be at the head of Suruga Bay (Ishibashi 2004), was revised to Cape Omaezaki by Matsu'ura (2012) on the basis of reports of low seismic intensity in Fujinomiya city, at the head of Suruga Bay (e.g., Kobayashi et al. 2018). The western edge of the rupture was at Cape Ashizuri in 1946 and 1854; however, in 1707 the northern part of the Hyuganada sector also ruptured (Furumura et al. 2011) (Fig. 2c). We emphasized the rupture extent in the strike direction, rather than the dip direction, to reproduce the rupture areas of the 1707 and 1854 earthquakes.

The seismic data for the 1944/1946 Showa earthquakes indicate that they initiated off Cape Shiono (Fig. 2a; target phenomenon 1e); however, researchers have made greatly differing estimates of their rupture areas (see Figs. 3–14–3–17 in Earthquake Research Committee 2013). Because Baba and Cummins (2005) achieved a better fit to the tsunami waveform data by adopting a more realistic plate configuration (similar to the one in this study) and by increasing the spatial resolution of the inversion, we adopted their solution to reproduce the rupture areas of the 1944/1946 Showa earthquakes (Fig. 2a). Note that we regarded the western edge of the Showa Nankai earthquake rupture to be on the eastern side of Cape Ashizuri (Fig. 1; Earthquake Research Committee 2013).

The great earthquakes before the 1707 Hoei earthquake are described in only a few historical records. For example, the 1605 Keicho earthquake has been called a tsunami earthquake, because it caused a disastrous tsunami but only weak seismic motion was reported, or possibly a teleseism (Earthquake Research Committee 2013). However, a recently discovered account from southeastern Shikoku (Tai 2006) describes an “unprecedented disaster by the great earthquake”, which suggests that the 1605 event may have been a typical Nankai Trough earthquake. Give the uncertainties for this event, we did not

(See figure on next page.)

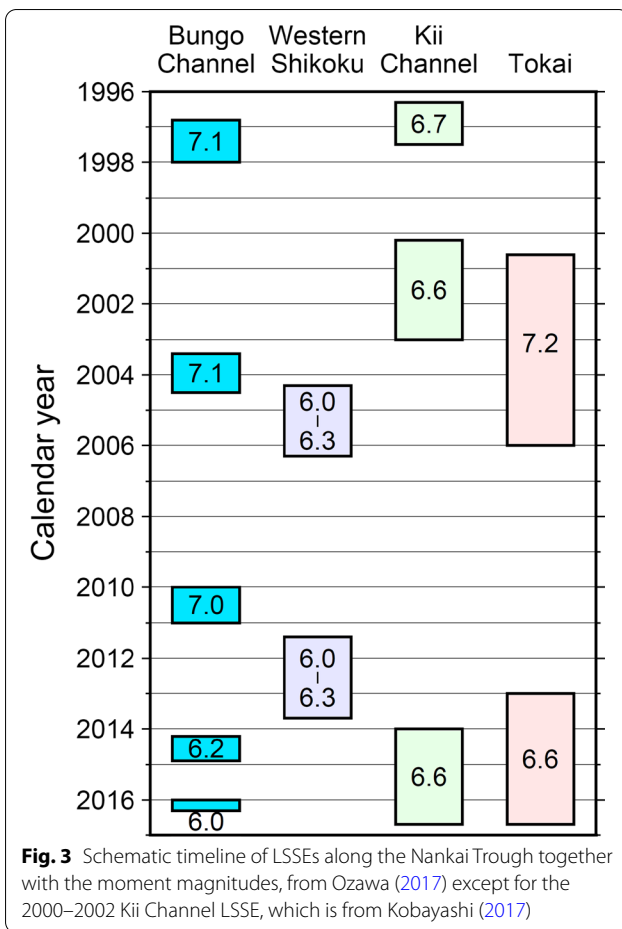
Fig. 2 Coseismic slips of historical earthquakes, slip-deficit rates, and gravity anomalies in the Nankai Trough region. **a** Areas of > 1 m inferred coseismic slip during the 1944 Tonankai (red) and 1946 Nankai (green) earthquakes (Baba and Cummins 2005), > 3 m slip during the 1946 Nankai earthquake (purple) (Murotani et al. 2015), and > 0.6 m slip during the 1968 Hyuganada earthquake (blue) (Yagi et al. 1998); colored stars indicate their epicenters. **b** Source segments of the 1854 Ansei Tokai (purple) and Nankai (brown) earthquakes whose amounts of average slips on segments are 4 m, 4 m, 4.6 m, and 6.3 m from the east (Aida 1981a, b). Blue outlines represent LSSE areas: (right to left) the 20-cm slip contour during 2001–2007 (Ozawa et al. 2016), the 4-cm slip contour during 2014–2017 (Kobayashi 2017), the ~6-cm contour of average slip during 2004–2005 (Takagi et al. 2016), and the 20-cm slip contour in 2003 (Geospatial Information Authority of Japan 2015). **c** Source of the 1707 Hoei earthquake whose amounts of average slips on segments are 5.6 m, 7.0 m, 5.6 m, 9.2 m, and 9.2 m from the east (Furumura et al. 2011); the easternmost area is doubtful (Matsu'ura 2012; Kobayashi et al. 2018). Broken gray lines are depth contours (10 km intervals) of the top of the subducting Philippine Sea plate (Hirose et al. 2008). **d** Slip-deficit rates (color) and direction of Philippine Sea plate motion (arrows) relative to the continental plate (Nishimura et al. 2018). The blue rectangle indicates the 2017–2018 LSSE (Yokota and Ishikawa 2020). Green dots indicate shallow VLFs (Takemura et al. 2019). Purple outlines, from right to left, enclose source regions of Tokai earthquakes (Central Disaster Management Council 2001) and Tonankai and Nankai earthquakes (Earthquake Research Committee 2001). **e** Free-air gravity anomalies. Thick black lines indicate a subducted seamount and ridges (Deep-Paleo: Kodaira et al. 2004; Paleo-Zenuis: Kodaira et al. 2004, Park et al. 2003; Tosabae: Kodaira et al. 2000; Kyushu-Palau: Yamamoto et al. 2013). Open arrows indicate ridges not yet subducted. **f** Regional tectonic map showing locations of the study area (red box) and the top panel of Fig. 1 (blue box)



aim to reproduce it with our model. Similarly, the 1498 Meio Tokai earthquake may have been an unpaired event because the occurrence of a 1498 Meio Nankai earthquake is doubtful (e.g., Ishibashi 1998).

The average recurrence interval of historical great earthquakes along the Nankai Trough was almost twice as long before the 1361 Shohei (Koan) earthquake as after it (Fig. 1), but the records may miss some events before 1361. Maemoku (1988) investigated an uplifted

assemblage of sessile marine organisms along the Cape Muroto coast and suggested that the 887 Nin'na and 1361 Shohei events (recurrence interval 474 years), but not the 1707 Hiei earthquake, were mega-earthquakes accompanied by unusual uplift. Shishikura et al. (2008), in a similar study along the southern coast of the Kii Peninsula, identified the 1361 and 1707 events as mega-earthquakes and estimated their recurrence interval to be 400–600 years. Okamura and Matsuoka (2012) investigated



tsunami deposits in lakes and marshes along the Pacific coast from Shikoku to Kyushu, and counting the 1707 Hoei, 1361 Shohei, and 684 Hakuho events as mega-earthquakes, they estimated the recurrence interval of mega-earthquakes to be 346–677 years. Thus, the recurrence interval of mega-earthquakes along the Nankai Trough has generally been inferred to be 400–600 years (target phenomenon 1d).

Because the seismic magnitude (Utsu magnitude) and tsunami magnitude differ for each earthquake (Earthquake Research Committee 2013), we adopted the range between these two magnitudes as our target magnitude for that earthquake (Table 1). Given their large errors, we disregarded estimates of rupture areas and recurrence intervals for events before the 1707 Hoei earthquake.

In the Hyuganada sector, no great earthquake occurred after the 1707 event until the M_w 7.5 event of 1968 in the northern Hyuganada area (blue outline in Fig. 2a; Yagi et al. 1998). We did not target the 1662 event in the Hyuganada sector (open star in Fig. 1) because its rupture area differed from that of the 1968 Hyuganada earthquake. Thus ~260 years (1707–1968) separates the historical

ruptures of the Hyuganada asperity (Fig. 1) (target phenomenon 2).

To detect and characterize interplate coupling, slip-deficit rates on the Nankai Trough plate boundary (target phenomenon 3) have recently been estimated by using land-based Global Navigation Satellite System (GNSS) data and offshore GNSS-Acoustic (GNSS/A) data (Yokota et al. 2016; Nishimura et al. 2018). This work defined several local maxima in slip-deficit rates, and identified offshore regions with relatively low slip-deficit rates off the Shima Peninsula, Cape Shiono, the southeastern coast of Cape Muroto, and Cape Ashizuri (Fig. 2d).

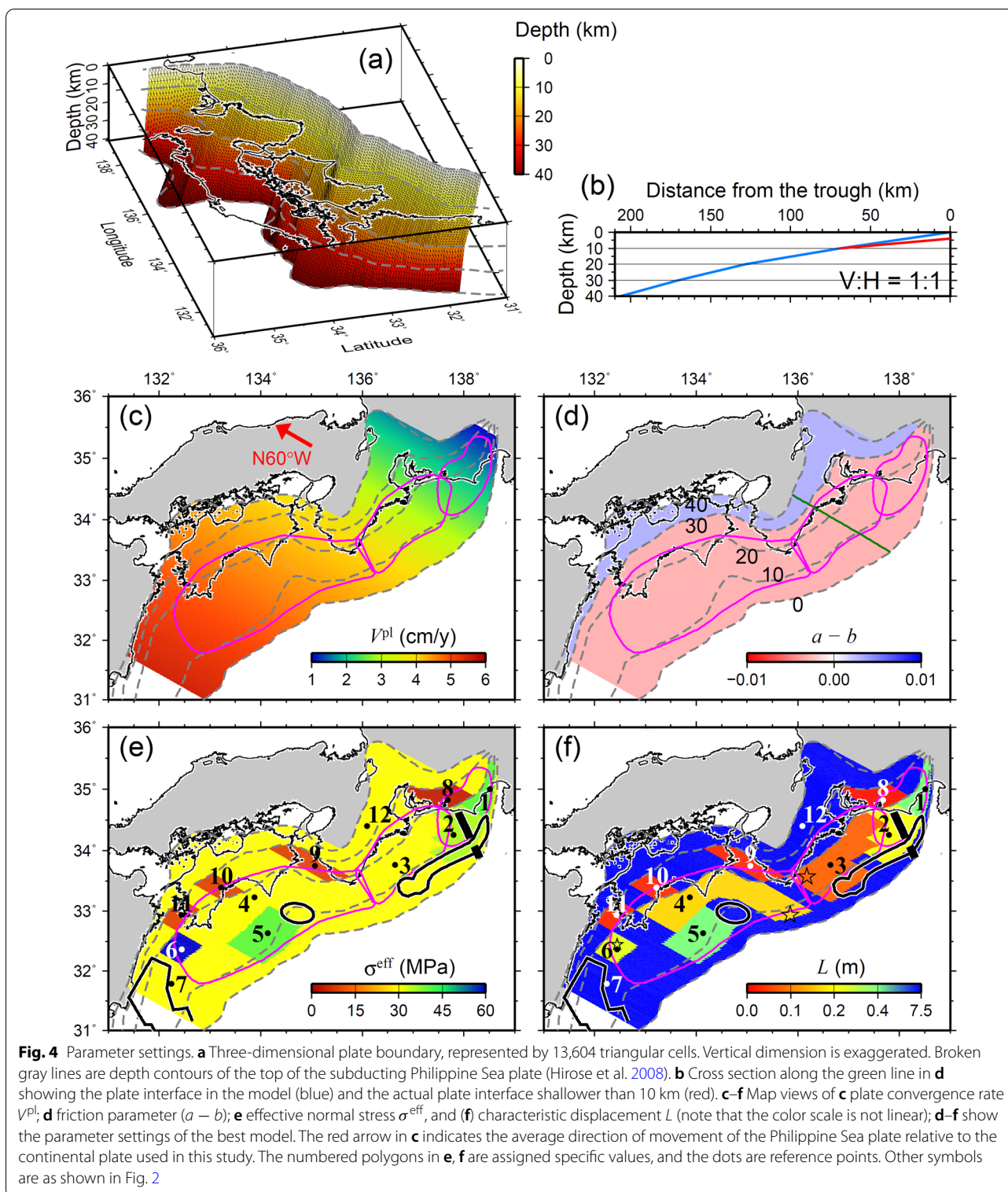
We sought to reproduce the recurring LSSEs (target phenomenon 4) in the Tokai district, Kii Channel, western Shikoku, and the Bungo Channel (Kobayashi 2014, 2017; Ozawa 2017) (Figs. 2b, 3). These differed in their average recurrence interval (~10 years in the Tokai district and the Kii Channel and ~6 years in western Shikoku and the Bungo Channel), average duration (~5 years in the Tokai district, ~2–3 years in the Kii Channel and western Shikoku, and ~1 year in the Bungo Channel), and magnitude (M_w ~7 in the Tokai district, M_w 6.5 in the Kii Channel, M_w ~6 in western Shikoku, and M_w 6–7 in the Bungo Channel). For western Shikoku LSSEs, where there was some variation in the slip distribution, our target event was an LSSE with an approximately square rupture area estimated from data recorded during October 2004 to October 2005 (Takagi et al. 2016). We omitted LSSEs in the Kyushu district (Ozawa 2017) because they had various recurrence intervals and we expected them to be very hard to reproduce.

Methods

Our model is a system of two plates in a uniform elastic medium that fills a 3-D half-space. We discretized the 3-D plate interface into triangular cells (Fig. 4a). In accordance with dislocation theory, shear stress on the plate interface is expressed as:

$$\tau_i^s(t) = \sum_{j=1}^N K_{ij} \left(V_j^{\text{pl}} t - u_j(t) \right) - \frac{G}{2\beta\eta} \frac{du_i(t)}{dt}, \quad (1)$$

where i and j are cell numbers, τ_i^s is shear stress in the i th cell, K_{ij} is the static shear stress in the center of the i th cell induced by a unit slip in the j th cell, V_j^{pl} and u_j are the plate convergence rate and slip amount in the j th cell, respectively, and t , G , and β are time, rigidity, and shear-wave velocity, respectively. η represents the correction factor of seismic radiation, which we set at 1 according to previous studies (e.g., Hori 2006; Hyodo and Hori 2013; Hirose and Maeda 2013; Nakata et al. 2014; Hyodo et al. 2016). Values of K_{ij} are obtained simply by using the dislocation stress formula, which is expressed in terms of



the Green’s function in a uniform elastic medium occupying a half-space (Mura 1987; Kuroki et al. 2002). The second term on the right-hand side of Eq. (1) represents the shear-stress reduction during high-speed slip. This

term was introduced by Rice (1993) to approximate quasi-dynamic slip behavior during earthquakes.

We assumed that frictional stress on the fault obeys an RSF law derived from laboratory experiments (Dieterich

1979, 1981; Ruina 1983), which describes the frictional stress on the i th cell as

$$\frac{\tau_i^f(t)}{\sigma_i^{\text{eff}}} = \mu_i(t) = \mu_0 + \Theta_i(t) + a_i \ln\left(\frac{V_i(t)}{V_0}\right). \quad (2)$$

Among the many versions of friction laws, we selected a composite law (Kato and Tullis 2001):

$$\begin{aligned} \frac{d\Theta_i(t)}{dt} = & \frac{V_0}{L_i} b_i \exp\left[-\left(\frac{V_i(t)}{V_c} + \frac{\Theta_i(t)}{b_i}\right)\right] \\ & - \frac{V_i(t)}{L_i} \left(\Theta_i(t) + b_i \ln\frac{V_i(t)}{V_0}\right). \end{aligned} \quad (3)$$

In this equation, τ_i^f , μ_i , σ_i^{eff} , Θ_i , and V_i are frictional stress, friction coefficient, effective normal stress, a state variable (Nakatani 2001), and slip velocity, respectively, in the i th cell. V_0 is an arbitrary reference velocity, set at 1.0×10^{-6} m/s. Parameter μ_0 is the steady-state friction coefficient at slip rate $V = V_0$ and is set at 0.6. V_c is the cut-off velocity for the composite law and is set at 1.0×10^{-8} m/s in accordance with Kato and Tullis (2001). Parameters a_i , b_i , and L_i are constant friction parameters that control sliding behavior on the fault. When $a - b < 0$ (velocity weakening), unstable slip may occur because strength decreases as slip velocity increases; thus, this condition represents a stick–slip area (asperity). When $a - b > 0$ (velocity strengthening), unstable slip does not occur unless it is driven by a strong stress perturbation; this condition represents a stable sliding area.

By assuming a quasi-dynamic equilibrium between shear stress and frictional stress and solving Eqs. (1)–(3) simultaneously, we derive the following differential equations related to stress and slip rate:

$$\frac{d\tau_i(t)}{dt} = \left\{ \frac{a_i}{V_i(t)} \sum_{j=1}^N K_{ij} (V_j^{\text{pl}} - V_j(t)) - \frac{V_0}{L_i} b_i \frac{G}{2\beta} \exp\left[-\left(\frac{V_i(t)}{V_c} + \frac{\Theta_i(t)}{b_i}\right)\right] - \frac{V_i(t)}{L_i} \frac{G}{2\beta} \left(\Theta_i(t) + b_i \ln\frac{V_i(t)}{V_0}\right) \right\} / \left(\frac{a_i}{V_i(t)} + \frac{G/\sigma_i^{\text{eff}}}{2\beta} \right), \quad (4)$$

$$\frac{dV_i(t)}{dt} = \left\{ \frac{1}{\sigma_i^{\text{eff}}} \sum_{j=1}^N K_{ij} (V_j^{\text{pl}} - V_j(t)) - \frac{V_0}{L_i} b_i \exp\left[-\left(\frac{V_i(t)}{V_c} + \frac{\Theta_i(t)}{b_i}\right)\right] + \frac{V_i(t)}{L_i} \left(\Theta_i(t) + b_i \ln\frac{V_i(t)}{V_0}\right) \right\} / \left(\frac{a_i}{V_i(t)} + \frac{G/\sigma_i^{\text{eff}}}{2\beta} \right), \quad (5)$$

$$\Theta_i(t) = \frac{\tau_i^f(t)}{\sigma_i^{\text{eff}}} - \mu_0 - a_i \ln\left(\frac{V_i(t)}{V_0}\right). \quad (6)$$

We integrated Eqs. (4)–(6) with respect to time by the fifth-order Runge–Kutta method with an adaptive step-size control (Press et al. 1992). The initial condition was $\tau_i(0) = \mu_0 \sigma_i^{\text{eff}} + (a_i - b_i) \sigma_i^{\text{eff}} \ln\left(\frac{V_i(0)}{V_0}\right)$ and $V_i(0) = 0.1 \text{ cm/y} (3.1688 \times 10^{-11} \text{ m/s})$ in all cells. For

simplicity, we considered only the component of fault movement in the direction of relative plate motion, and we considered the variation of static shear stress on the fault only in this direction; we also assumed that the effective normal stress was constant in time (see Sect. 6.4). Note that Eq. (1) assumes constant slip at the plate convergence rate outside as well as inside the study area.

We defined a period with slip of more than 0.1 m/s in a cell as an earthquake term. We estimated M_w by using the relationship $\log M_0 = 1.5 M_w + 9.1$ (Kanamori 1977), where M_0 (Nm) is obtained from the total amount of slip during the coseismic term.

Our simulations used 100 virtual nodes (1.1648 TFLOPS/node) of the FUJITSU Server PRIMERGY CX2550 M1 server node with message passing interface (MPI) and automatic parallelization. A single simulation run of 5500 years (1 million steps) required about 18 h of calculation time. We set parameters through trial and error and conducted 190 simulation runs.

Previous simulations of great Nankai Trough earthquakes

Here, we review several previous earthquake cycle simulations based on the RSF law that have been conducted to investigate the occurrence patterns of great Nankai Trough earthquakes.

Hori (2006), using a planar subduction model with frictional parameters based on marine seismic survey results, qualitatively reproduced the recurrence interval variations and time lags between Tokai/Tonankai and Nankai earthquakes for the three most recent events. However, the model results differed from the historical records quantitatively.

Hyodo and Hori (2013) extended the study area of Hori (2006) to the Trough axis and then set large L values, corresponding to large fracture energy near the Trough axis. Their simulation produced an M_w 9-class megathrust earthquake that ruptured the entire seismogenic layer, including shallow areas, in a cycle of about 370 years and an M_w 8.6 event that ruptured a plate boundary at depths of 10–30 km in a cycle of about 200 years.

Hirose and Maeda (2013) successfully simulated the non-rupture of the Tokai segment during the 1944 Tonankai earthquake as well as the recurring LSSEs observed in the Tokai region by setting frictional parameters in their 3-D model represent the subducting seamounts off the Tokai district and dehydration reactions beneath the Lake Hamana area. Earthquake cycles in their model results were very simplified, and the time lag between the simulated Tokai/Tonankai and Nankai earthquakes was not consistent with the historical record.

Nakata et al. (2014) simulated Nankai Trough events from Cape Shiono to southern Kyushu, reproducing the 1968 Hyuganada earthquake and LSSEs in the Bungo Channel, and then investigated the influence of these events on Nankai earthquakes. However, because their study area did not include segments east of Cape Shiono, their model implicitly assumed constant slip at the rate of plate convergence on these segments, on which the plate boundary is actually locked (Nishimura et al. 2018).

Hyodo et al. (2016) extended the study area of Nakata et al. (2014) to include the Tokai region and investigated the influence of Hyuganada earthquakes on Nankai earthquakes in simulations using the parameter settings of Hori (2006) and Nakata et al. (2014). Their results showed that Hyuganada earthquakes tended to trigger Nankai earthquakes within several years. Although they also suggested that the 1498 Meio Nankai earthquake might have been triggered by a Meio Hyuganada earthquake, the occurrence of both of these earthquakes is doubtful (Ishibashi 1998; Harada et al. 2017). In addition, their model did not reproduce the non-rupture of the Tokai segment in 1944.

Because all of these simulation studies focused on particular phenomena, a comprehensive investigation of seismic phenomena in the Nankai Trough has yet to be achieved.

Modeling parameters

In this section, we describe the parameters of the best model we obtained through parameter tuning (Fig. 4; Table 2). See Section S2 in the Additional file 1 for details of the parameter tuning.

Plate configuration

We modeled the 3-D plate interface from the Tokai region to southern Kyushu to a depth of 40 km (Fig. 4a) by expanding the model area of Hirose and Maeda (2013) and covering the resulting surface with triangular cells.

The Nankai Trough axis lies 4–5 km below sea level, posing challenges for modelers. When the free surface in the elastic half-space model is set to sea level, the tip of the plate boundary is buried within the elastic body. In this case, slip on the plate boundary could cause unrealistic stress concentrations at the tip (Hyodo and Hori 2013), even if the relationship between land-based GNSS locations and the plate boundary is realistic. When the free surface is set to the depth of the trough, coinciding with the tip of the plate boundary, it becomes hard to compare simulations based on land-based GNSS data and offshore GNSS/A data because crustal deformation cannot occur in the air. Furthermore, in this case, the shallow slip becomes unrealistically large, and the rupture becomes difficult to stop (Hyodo et al. 2016). Each approach has advantages and disadvantages. To avoid their disadvantages, we used the plate configuration of Hirose et al. (2008) for depths below 10 km, set the depth of the Trough axis to 0 km, and for depths shallower than 10 km connected the trough axis linearly to the plate interface at 10 km depth (Fig. 4a, b), similar to the configuration used by Hirose and Maeda (2013). Note that in this model, the $\sim 8^\circ$ dip angle of the plate interface

Table 2 Parameters in our best simulation model at points 1–12 in Fig. 4e, f

Point (Fig. 4e, f)	L (m)	σ^{eff} (MPa)	h^* (km)	a	b	$a-b$
1	0.4000	40	100.0	0.005	0.008	– 0.003
2	0.2200	35	62.9	0.005	0.008	– 0.003
3	0.0800	30	26.7	0.005	0.008	– 0.003
4	0.1700	30	56.7	0.005	0.008	– 0.003
5	0.6000	40	150.0	0.005	0.008	– 0.003
6	0.2400	60	40.0	0.005	0.008	– 0.003
7	7.5000	30	2500.0	0.005	0.008	– 0.003
8	0.0150	5	30.0	0.005	0.008	– 0.003
9	0.0335	10	33.5	0.005	0.008	– 0.003
10	0.0335	10	33.5	0.005	0.008	– 0.003
11	0.0335	10	33.5	0.005	0.008	– 0.003
12	7.5000	30	–	0.005	0.002	0.003

at depths shallower than 10 km is slightly larger than the actual $\sim 6^\circ$ dip angle.

We arranged the model cells in the plate configuration as follows. First, we set the y -axis in the $N60^\circ W$ direction (red arrow in Fig. 4c) according to the average subduction direction estimated by Nishimura et al. (2018), the x -axis in the $N150^\circ W$ direction orthogonal to the y -axis, and the z -axis in the depth direction. We arranged 138 strips in the x -axis direction, each 5 km wide parallel to the y -axis, that are linearly connected between the 0, 10, 20, 30, and 40 km depth contours. Then, we laid triangles with edges ~ 5 km long edge to edge (not overlapping) over the inside of the strip in the dip direction, to yield a 3-D plate configuration consisting of 13,604 triangular cells.

For simplicity, we fixed the direction of plate convergence to $N60^\circ W$ (red arrow in Fig. 4c). We used a plate convergence rate of 5.5 cm/y in the western part of the study area and decreased to 1.0 cm/y at the eastern edge of the study area (Nishimura et al. 2018) (Fig. 4c). Although rigidity and shear-wave velocity generally increase with depth, we determined elastic moduli using $G = 30$ GPa, a Poisson's ratio of 0.25, and $\beta = 3.75$ km/s according to previous studies (Hori 2006; Hyodo and Hori 2013; Hirose and Maeda 2013; Nakata et al. 2014; Hyodo et al. 2016). The S-wave velocity of 3.75 km/s corresponds to the depth of 20 km in the JMA2001 one-dimensional velocity structure (Ueno et al. 2002).

Computational instability due to cell size

Rice (1993) derived the critical nucleation size h^* required to satisfy the continuum approximation and demonstrated that the computation cell size h must be smaller than h^* . For the i th cell, h/h^* is given theoretically by $(b_i - a_i)\sigma_i^{\text{eff}}/L_i K_{ii}$ (Hori et al. 2004). In our simulations, the maximum h/h^* was 0.12 on the Tonankai segment (the segment including point 3 in Fig. 4f). Liu and Rice (2005) showed that values of h/h^* between 0.25 and 0.125 have minimal effect on simulated slip displacements and slip rates. Shibazaki et al. (2019) performed cycle simulations in a 3-D model with another nucleation length scale $L_b \approx GD_c/b\sigma_n^{\text{eff}}$ (Dieterich 1992; Rubín and Ampuero 2005) of 4.7 km for the seismogenic zone and noted that in the seismogenic zone there were typically 15 grid points within a region with a 4.7-km radius, ensuring good resolution. In our study, there were typically 25 grid points in a region with a 10.0-km radius corresponding to the minimum L_b in the seismogenic zone (point 3 in Fig. 4f). Therefore, we believe that the resolution of our numerical model is sufficient for evaluating the occurrence patterns of great earthquakes and LSSEs. Although the critical fault length l_c is expected to change according to the aspect ratio of a rectangular asperity (which is

suggested by the slip and stress relation expressed by for example (A6) in Kato (2003)), we approximated the critical fault length by h^* because the asperities in our 3-D model are not simple circles or rectangles.

Tuning of friction parameter $a - b$

The seismogenic zone on the Nankai Trough plate boundary has an estimated depth range of 10–30 km (Hyndman et al. 1995). However, because coseismic slip off Cape Shiono appears to extend up to the trough axis (Sakaguchi et al. 2011), we set $a - b < 0$ above 30 km and $a - b > 0$ in the stable sliding area below 30 km (Fig. 4d). This setting differs from Hirose and Maeda (2013), who set $a - b > 0$ from 10 km depth to the trough axis.

Frictional parameters a and b depend on depth (Blanpied et al. 1998). To simplify our analysis, we set frictional parameter a to a constant value of 0.005, similar to results from friction experiments (Sawai et al. 2016), and we changed b at 30 km depth by a step function (Fig. 4d; Table 2). Previous studies have tended either to assign $a - b < 0$ to seismic asperities and $a - b > 0$ for other areas (e.g., Shibazaki et al. 2011) or to assign $a - b$ values according to depth (e.g., Nakata et al. 2016; Hirose and Maeda 2013). We followed the latter approach in this study. Because the recurrence interval of earthquakes is generally proportional to the product $(b - a)\sigma^{\text{eff}}$ and characteristic displacement L in the seismogenic zone (e.g., Stuart 1988), we determined a value of -0.003 for $a - b$ by trial and error until the model simulated the historical record.

After fixing the spatial distributions of plate convergence rate V^{pl} and $a - b$ (Fig. 4c, d), we tuned the spatial distributions of effective normal stress σ^{eff} and characteristic displacement L as described in the next two sections. Although we strove for simplicity, the parameter distributions that reproduced the target phenomena were complicated (Fig. 4e, f) (see Additional file 1: Section S2). This result differs from that of Hirose and Maeda (2013) in that our parameter distribution was heterogeneous in areas outside the Tokai region. Note that although $a - b$ was constant over the 0–30 km depth range, the heterogeneity of σ^{eff} meant that the friction parameter $(b - a)\sigma^{\text{eff}}$, which characterizes the behavior of slip, was likewise heterogeneous.

Tuning of effective normal stress σ^{eff}

Effective normal stress can be described by $\sigma^{\text{eff}} = \sigma_r - \sigma_p$, where σ_r is lithostatic pressure and σ_p is pore pressure. If rock density ρ_r is assumed to be $2.8 \times 10^3 \text{ kg/m}^3$, then lithostatic pressure over the 10–30 km depth range is 274–823 MPa, from $\sigma_r = \rho_r g z$, where g is gravitational acceleration (9.8 m/s^2) and z is depth. Hydrated minerals in oceanic crust liberate large

amounts of water when they undergo phase transformations at depth (Hacker et al. 2003). This fluid release increases the pore pressure and reduces the effective normal stress at the plate boundary. Estimated pore pressure ratios σ_p/σ_r in the Nankai Trough are high at 0.92–0.98 (Seno 2009; Okamoto et al. 2016; Suenaga et al. 2016), indicating that σ^{eff} is 5–66 MPa at depths of 10–30 km. We adopted 30 MPa as the standard value for σ^{eff} (yellow in Fig. 4e) because we did not know how it changes in the dip direction. Note that Hirose and Maeda (2013) set σ^{eff} at 100 MPa, following the high pore pressure model of Rice (1992) adopted at the San Andreas Fault.

However, a fixed σ^{eff} value of 30 MPa did not enable us to reproduce target phenomena 1a, 1d, and 2, so we allowed σ^{eff} (and L) to be heterogeneous. Seafloor ridges and seamounts on the Philippine Sea plate correspond to positive gravity anomalies, and similar seamounts have been documented on the surface of the subducted slab, Paleo-Zenisu and deep-Paleo ridges (Park et al. 2003; Kodaira et al. 2004) (Fig. 2e). The subducting seamount (Tosabae) southeast of Cape Muroto (Kodaira et al. 2000) also corresponds to a positive gravity anomaly (ellipse in Fig. 2e). A similar anomaly can be seen near the trough axis off Shikoku (rectangle with dashed line in Fig. 2e) and near the coast of Shikoku, although a corresponding seamount has not been found. Because subducting seamounts increase the normal stress (Scholz and Small 1997), it is thought that the seamount behaves as a barrier or asperity due to strengthening interplate coupling (Yang et al. 2012). There are also contrary indications that a subducting seamount does not itself become an asperity and that stable sliding occurs along its trace (Tsuru et al. 2002; Mochizuki et al. 2008). Yokota et al. (2015) pointed out from the observation of GNSS/A that the interplate coupling may have been strengthened by Paleo-Zenisu ridge, but decreased by Tosabae off Cape Muroto. The occurrence of a shallow very low frequency earthquake (VLFE) (Takemura et al. 2019) coinciding with the Tosabae seamount indicates the presence of fluid southeast of Cape Muroto, so effective normal stress at Tosabae may not be high even in seamounts. Thus, the effect of seamounts is under debate. Accordingly, we specified higher σ^{eff} (35–40 MPa) where seamounts are subducting off Tokai (points 1 and 2 in Fig. 4e). This step enabled us to partially reproduce target phenomenon 1a, diversity at the eastern end of the Tokai/Tonankai sector (see Sects. 6.1.1, 6.1.2, and Additional file 1: S2). Although the relationship between the positive gravity anomaly off Shikoku and the seamounts is not clear, we assigned the standard σ^{eff} value (30 MPa) in the coastal area of Shikoku (the slip area of the 1946 Nankai earthquake in Fig. 2a) ruptured every time by a great earthquake (Figs. 1, 2) to reproduce the short recurrence interval,

but high σ^{eff} value (40 MPa) in the area far off Shikoku (point 5 in Fig. 4f) to reproduce infrequent rupture. We assigned the standard σ^{eff} value (30 MPa) in Tosabae area taking the above-mentioned discussion into consideration. These steps enabled us to reproduce the recurrence interval of mega-earthquakes (target phenomenon 1d) and low slip-deficit rate southeast of Cape Muroto (target phenomenon 3). For the asperity in northern Hyuganada, we assigned a high σ^{eff} value of 60 MPa (point 6 in Fig. 4e) to reproduce the long recurrence interval of ~260 years (target phenomenon 2).

The occurrence of LSSEs indicates the presence of larger amounts of fluid (Hirose et al. 2008) and higher pore pressures (lower σ^{eff}) than in surrounding areas. Therefore, we assigned lower σ^{eff} values to the LSSE areas than to surrounding areas (Fig. 4e) to reproduce these LSSE areas, using trial and error to make the recurrence interval of LSSEs consistent with observations (target phenomenon 4) and taking into consideration the difference in plate convergence rates in the east–west direction. At the same time, we tuned the LSSE amplitudes by values of L (see below).

Tuning of characteristic displacement L

Characteristic displacement L has been estimated by laboratory experiments to be a few micrometers (e.g., Dieterich 1979). However, L in real fault systems ranges from centimeters to meters (e.g., Guatteri et al. 2001; Hirose and Bystricky 2007). And because L increases with fault roughness (Dieterich 1979), L is expected to be large in areas where subducted seamounts are present on the plate boundary. A large L acts as a barrier to rupture (e.g., Hirose and Maeda 2013).

The 1944/1946 Showa earthquakes (Baba and Cummins 2005) are thought to have also ruptured during the 1854 Ansei and 1707 Hoei earthquakes (Fig. 2), establishing a short recurrence interval. Accordingly, from Stuart (1988), we considered it appropriate to set smaller L values in the Showa earthquake slip areas (including points 3 and 4 in Fig. 4f). In addition, we made L smaller east of Cape Shiono (point 3) than west of the cape (point 4) in consideration of the fact that the Tonankai side tends to rupture before the Nankai side. We assigned large L to a belt off Cape Shiono to impose a barrier between the Tonankai and Nankai rupture areas and reproduce the time lag between their ruptures (target phenomenon 1c). A seismic survey revealed the existence of a structural boundary of the subducting Philippine Sea plate's crust off Cape Shiono (Mochizuki et al. 1998). The belt-shaped area of large L assigned in this study may be related to the structural boundary of the slab crust. If the critical nucleation size h^* is sufficiently large due to the large L , stable sliding occurs without nucleation even in regions where

$a - b < 0$ (Kato 2003). Since this setting also promotes a stable sliding, it also helps reproduce the low slip-defect rate off Cape Shiono (target phenomenon 3) (Fig. 2d). Similarly, we assigned large L values to regions off the Shima Peninsula (between areas including points 2 and 3 in Fig. 4f), southeast of Cape Muroto (Tosabae), and off Cape Ashizuri (between points 4 and 6) where low slip-deficit rates were identified (Fig. 2d). In the regions where σ^{eff} had values other than 30 MPa (Fig. 4e), we reproduced the along-strike extent of the rupture area (target phenomenon 1a), the 400–600 year recurrence interval of mega-earthquakes (target phenomenon 1d), and the Hyuganada seismic gap (target phenomenon 2) by assigning larger L values for points 1, 2, 5, and 6 than for points 3 and 4, and we assigned smaller L values for points 8–11 to reproduce the repeating LSSEs (target phenomenon 2). Then we assigned large L values (7.5 m) to the surrounding regions according to the hierarchical asperity model of Hori et al. (2009) and Hyodo and Hori (2013), in which an area of small L is surrounded by an area of large L that can serve as a barrier and an asperity. Hyodo and Hori (2013) correlated L with fracture energy. We also assigned a large L value to the southern Hyuganada sector (point 7) to reproduce stable sliding, rather than nucleation, even though $a - b < 0$, because the interplate coupling rate there is low (Yamashita et al. 2012).

Yokota and Ishikawa (2020) documented multiple LSSEs with a duration of about 1 year around GNSS/A sites. Of these, the LSSE of 2017–2018 (M_w 6.6) was near the trough axis at 134.5–136°E off the Kii Peninsula, and it corresponded closely with VLFE activity (Fig. 2d). Other possible LSSEs were observed at GNSS/A sites near VLFE regions in the shallow part of the plate boundary, and interplate coupling is considered to be weaker near the trough axis than in the seismogenic zone. This study did not attempt to reproduce these shallow LSSEs, but the effect a large L value along the trough axis (Fig. 4f) is thought to weaken interplate coupling.

Results and discussion

In this section, we present and discuss the simulation results for the Nankai Trough plate boundary based on the best parameter distributions (Fig. 4; Table 2). To avoid the effect of initial values, we show only events after the first 600 years of the 5000-year simulation. We add the prefix “S” to elapsed time from the start of the simulation to avoid confusion with calendar dates. During S600–S5000, our simulation produced 106 seismic events with M_w between 6 and ~ 8.5 and repeating LSSEs (Additional file 1: Figs. S2 and S3). Among seismic events, 66 were great earthquakes or mega-earthquakes ($M_w \sim 8$ or higher), 31 were earthquakes of $M_w \sim 7.5$ in northern

Hyuganada, and 9 were earthquakes of M_w 6-class in LSSE areas.

Earthquakes

Representative slip distributions

We used rupture patterns to classify our simulated 66 earthquakes of $M_w \sim 8$ or higher into the following six types (Fig. 5). Nine of them events could not be classified as one of these:

1. The “Showa type” is a pair of earthquakes with epicenters off Cape Shiono in which the deeper parts of segments A and B rupture in an M_w 8.0–8.1 event within 3 years after segments C and D rupture in an M_w 7.9–8.1 event.
2. The “Ansei type” is a pair of earthquakes in which segments A and B rupture in an M_w 8.3–8.4 event within 0.1 year after segments C–F rupture in an M_w 8.3–8.4 event.
3. The “Hoei type” is the simultaneous (within 0.03 years) rupture of segments A–E in an M_w 8.4–8.6 event and segment Z in an $M_w \sim 7.5$ event.
4. The “quasi-Showa type” is the same as the Showa type but includes a rupture in the shallower part of segment A.
5. The “quasi-Hoei type” is the same as the Hoei type but includes a rupture of segments Z–E within 0.03–1 years.
6. The “isolated Tonankai type” is an M_w 8-class Tonankai event (segments C and D) without an M_w 8-class Nankai event (segments A and B) within several tens of years.

Following are some considerations that affected our definitions. Although the historic Ansei Tokai and Nankai earthquakes were about 32 h apart, in the definition of Ansei-type earthquakes we allowed the time lag to be as long as 0.1 year. With respect to Showa-type events, Baba and Cummins (2005) used tsunami data to estimate that the main rupture area of the 1946 Showa Nankai earthquakes was near the coast, and we targeted that area (target phenomenon 1e); however, the joint inversion analysis by Murotani et al. (2015) using seismic waveforms and geodetic data showed that an area of large slip on the Nankai segment amounting to M_w 8.4 was farther offshore. Accordingly, we defined an event with rupture area including offshore with magnitude less than M_w 8.4 as a quasi-Showa-type earthquake. With respect to Hoei-type events, the 1707 Hoei earthquake rupture may not have extended eastward to segment F (Matsu’ura 2012); thus, it may be reasonable to add the possibility that segments E and F remain unruptured to the definition of a Hoei-type earthquake given the low resolution of rupture

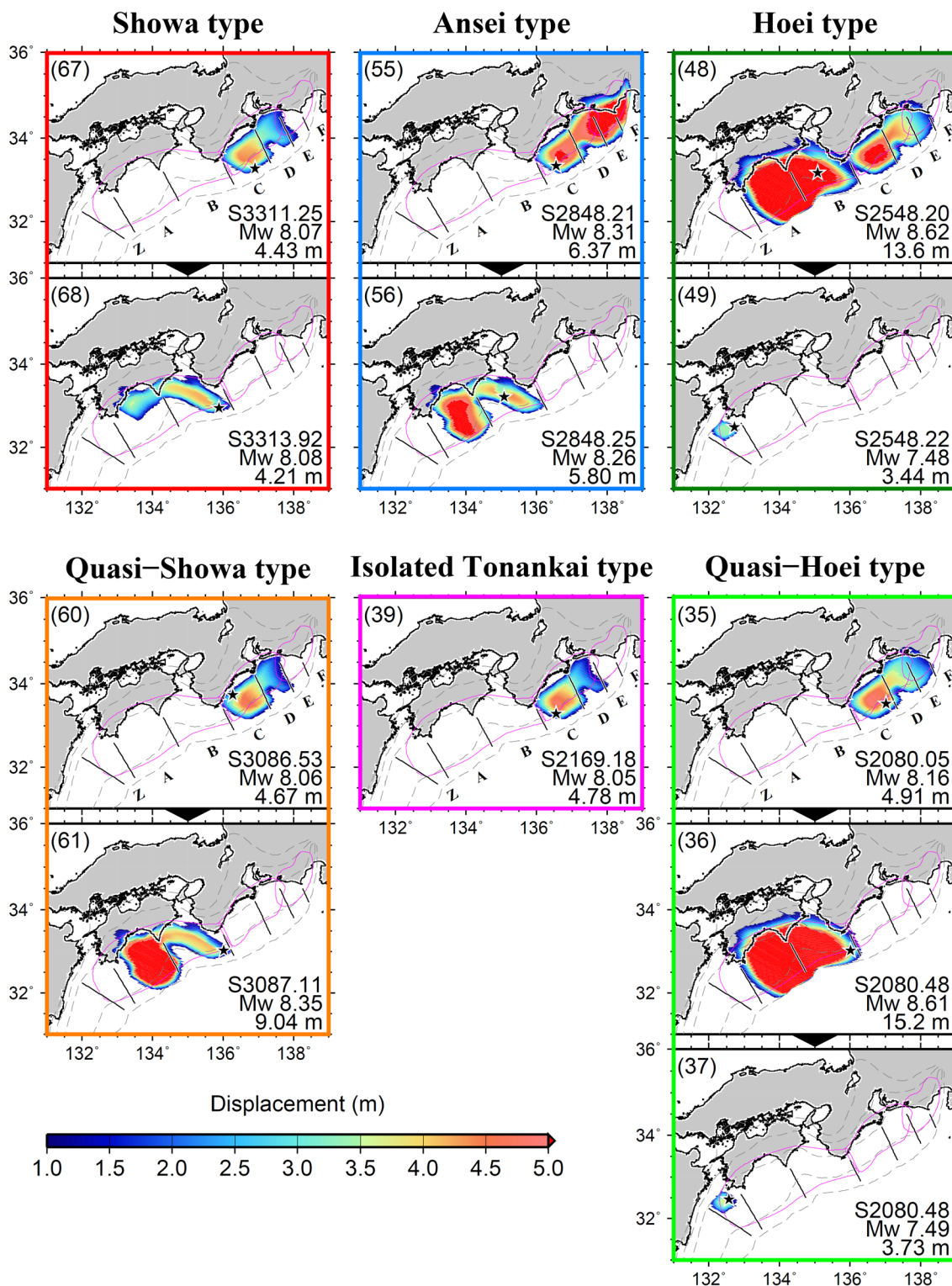


Fig. 5 Examples of slip distribution in six types of earthquake events in our 4400-year simulation. Stars indicate rupture initiation points. In each plot, the event number is at upper left (see Additional file 1: Fig. S2 for all 106 numbered events), and the numbers at lower right are the elapsed years in the simulation (S600–S5000), the moment magnitude, and the maximum slip displacement. Colors of the borders correspond to the event type

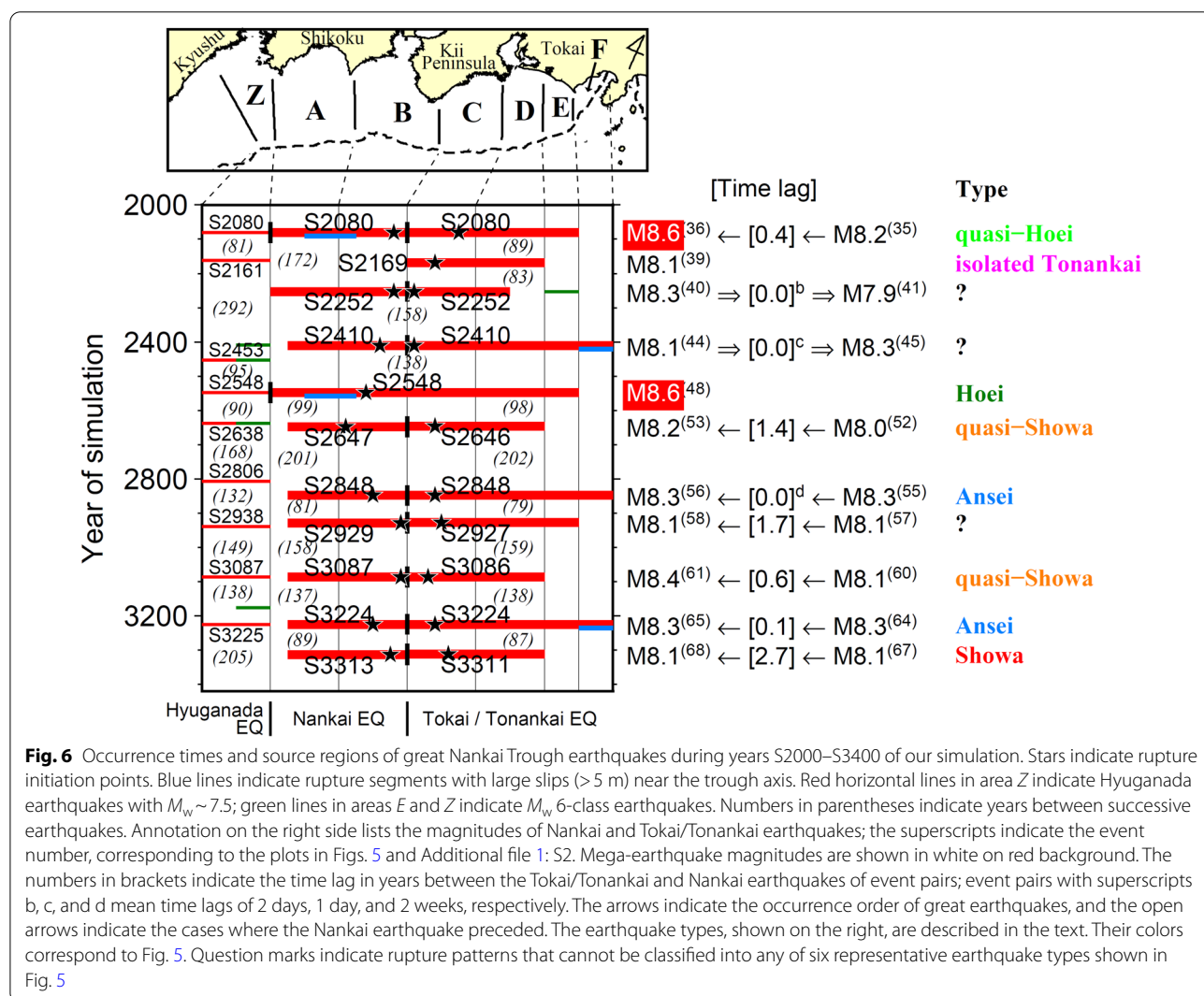
areas inferred from historical documents. We therefore defined a rupture of segments Z–D or Z–E of magnitude $M_w \geq 8.5$ within 1 year as a quasi-Hoei-type earthquake, although the recorded time lag between the Hoei Tokai/Tonankai and Nankai earthquakes is extremely short (Imai et al. 2011).

Figure 6 shows the simulated earthquakes during S2000–S3400, and Additional file 1: Figs S2 and S3 show events for the whole simulation period (S600–S5000). Our model showed that events east and west of Cape Shiono tend to occur in pairs, sometimes simultaneously but usually with time lags between them. The individual rupture areas of these paired events generally showed considerable variation (target phenomenon 1a), but even when two event pairs had identical rupture areas, they differed in their maximum displacements and moment magnitudes (compare events 23–24 and 32–33 in Additional file 1: Fig. S2).

Great earthquakes

Our model simulated six Showa-type earthquakes and reproduced the epicenters and rupture areas of the 1944 and 1946 Showa earthquakes as estimated from tsunami data (Baba and Cummins 2005) (compare the Showa type in Figs. 5 and 2a). There were eight quasi-Showa-type earthquakes. There were six Ansei-type earthquakes, and our model roughly reproduced the coseismic slip area of the 1854 Ansei earthquake pair (Aida 1981a, b) (compare Figs. 5, 2b). There were two Hoei-type earthquakes, and our model roughly reproduced the coseismic slip area of the 1707 Hoei earthquake (Furumura et al. 2011; Mats’ura 2012; Kobayashi et al. 2018) (compare Figs. 5 and 2c). There were three quasi-Hoei-type earthquakes.

The sequence of events 95–103 in S4572–S4799 (Additional file 1: Figs. S2 and S3) was generally consistent with observations in terms of the event order and slip areas of the historical (Hoei, Ansei, and Showa)



earthquake sequences, if the quasi-Hoei type is included. In this sequence, great earthquakes had occurrence intervals of 137 and 86 years, similar to the historical intervals of ~150 and 90 years (target phenomenon 1b). The interval between events of the Showa-type pairs (events 102 and 103) in the simulation was 2.6 years, which is consistent with the historical interval of ~2 years (target phenomenon 1c). Although the interval between events in the simulated Ansei-type pairs (events 99 and 100) differed from the historical record by an order of magnitude (0.1 y in the simulation vs. 32 h), the simulation is qualitatively consistent with the historical record in that the difference was shorter for Ansei-type than for Showa-type event pairs (target phenomenon 1c). However, the interval between the quasi-Hoei-type event pair (events 95 and 96) was 0.7 years, which is longer than the 0.1-year interval of the Ansei-type pairs.

The 66 great earthquakes included 31 pairs in which events east and west of Cape Shiono were separated by 4.5 years or less. Among these pairs, the eastern event occurred first in 28 pairs and the western event occurred first in 3 pairs (events 12 and 13, events 40 and 41, and events 44 and 45 in Additional file 1: Fig. A). In addition, three events had simultaneous ruptures of both the east and west sides of Cape Shiono (events 10, 15, and 48 in Additional file 1: Fig. S2). Each of these three events initiated west of Cape Shiono, and their magnitudes were M_w 8.5–8.6. One event, an M_w 8.1 isolated Tonankai earthquake (event 39 in Additional file 1: Fig. S2) may be regarded as similar to the 1498 Meio Tokai earthquake, because the existence of its western counterpart is doubtful (e.g., Ishibashi 1998).

Earthquake Research Committee (2013) evaluated the occurrence potentials of Nankai Trough earthquakes with the use of a time-predictable recurrence model (Shimazaki and Nakata 1980). Hashimoto (2022) reexamined the long-term evaluation of the occurrence of great earthquakes along the Nankai Trough issued by Earthquake Research Committee (2013) and related materials, and found several problems in the adoption of the time-predictable model (e.g., neglect of measurement errors of uplift during historical earthquakes; inconsistency between assumed uplift and geodetic or geomorphological data). Thus he recommended to adopt a simple average of recurrence intervals instead of the time-predictable model to calculate the probability of the next earthquake. Horii et al. (2012) showed a time-predictable behavior in a simple hierarchical asperity model consisting of two small patches, but also pointed out that the behavior did not necessarily appear in general. Figure 7 shows the cumulative slip displacements at points 1–5 in Fig. 4f. The Tonankai asperity (area including point

3), where ruptures tended to initiate first, fit neither the time-predictable nor slip-predictable models. Therefore, it appears that the recurrence interval changed in response to local differences in stress conditions in surrounding asperities. The slip-predictable model was a better fit for the other four asperities (although the point 1 asperity was rather periodic), which tended to slip in

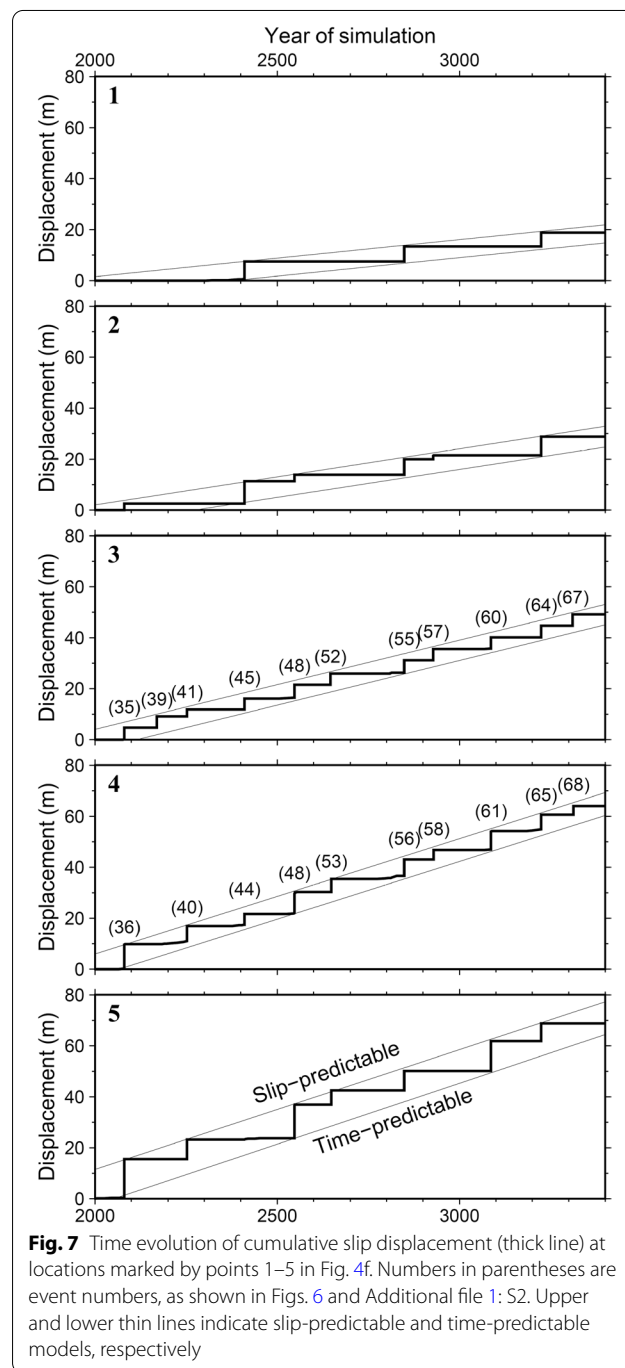


Fig. 7 Time evolution of cumulative slip displacement (thick line) at locations marked by points 1–5 in Fig. 4f. Numbers in parentheses are event numbers, as shown in Figs. 6 and Additional file 1: S2. Upper and lower thin lines indicate slip-predictable and time-predictable models, respectively

association with ruptures of adjacent asperities. From these results, when discussing the probability of occurrence of the next great earthquake, it is important to evaluate without persisting in the time-predictable model.

Mega-earthquakes

The 1707 Hōei earthquake, at M_u 8.6, is generally considered to be the largest known earthquake in the Nankai Trough (Table 1). Our simulation produced eight mega-earthquakes (events 2, 10, 15, 26, 36, 48, 88, and 96 in Additional file 1: Fig. S2), with occurrence intervals of 287–1654 years, and the average interval of 560 years is similar to the recurrence intervals of 400–600 years (target phenomenon 1d) estimated from field investigations (Maemoku 1988; Shishikura et al. 2008; Okamura and Matsuoka 2012). The slip was large in the area of the subducting seamount southeast of Cape Muroto with the low slip-deficit rate, even when we assigned the area a large L value to produce stable sliding.

We also examined events with large slips (>5 m) near the trough axis (blue lines in Figs. 6 and Additional file 1: S3). About 40% (=4/11) of the Tokai/Tonankai events that ruptured segment F reached the trough axis. Slips were large at the trough axis when the area with large σ^{eff} (point 5 in Fig. 4e) and the area with the subducting seamount (Tosabae) both ruptured (e.g., event 88 in Additional file 1: Fig. S2; compare events 85, 88, 90; event 85 did not rupture both areas and event 90 ruptured point 5 but not the Tosabae seamount).

Our findings also offer insight into the role of deep locked zones. Okamura and Shishikura (2020) proposed, based on geological data on crustal movements of the forearc wedge, that the 1854 Ansei Tokai earthquake was ruptured with the deep locked zone at ~20 km depth beneath the Akaishi Mountains in the Tokai region, whereas the 1944 Showa Tonankai and 1946 Showa Nankai earthquakes did not rupture the deep locked zone. With respect to this proposal, we were able to reproduce the variations in the eastern end of the ruptures of historic (1707, 1854, and 1944) earthquakes by setting barrier-like asperities with larger σ^{eff} and h^* at 5–20 km depth in the area including points 1 and 2 in the Tokai district (Fig. 4e, f). They also proposed that mega-earthquakes with a recurrence interval of 400–600 years, such as the 1707 Hōei earthquake, are controlled by the locked zone at 20–30 km depth beneath the Kii Mountains in Kii Peninsula. However, our simulation reproduced mega-earthquakes by setting barrier-like asperities in the area including point 5 off Shikoku. The placement of a strong locked zone beneath the Kii Mountains is an open question.

Time lag between Tokai/Tonankai and Nankai earthquakes

The Working Group to Investigate Disaster Prevention Based on Monitoring and Assessment of Seismicity along the Nankai Trough (2017) considered the possibility of pairs of great earthquakes occurring in close succession on opposite sides of Cape Shiono. The working group found that among the 96 events of M_w 8.0 or more that occurred worldwide after 1900, 10 were followed within 3 days by an earthquake of the same magnitude in an adjacent region. They showed that this fraction of event pairs could be approximated by the Omori–Utsu equation (Utsu 1961).

Our simulation produced 34 pairs of Tokai/Tonankai and Nankai great earthquakes on adjacent fault segments, of which 3 were simultaneous and 30 involved a time lag of less than 3 years (1 pair, events 30 and 31, had a time lag > 3 year). The time lags tended to cluster around peaks at several days and 0.1, 0.4, 0.7, and 2.6 years (Additional file 1: Fig. S3), a result that is inconsistent with the Omori–Utsu equation (Utsu 1961). Our model may simply differ from that equation in this respect, or there may be time lags that are inherent in the Nankai Trough region. Although the sample size is very small, the four historical earthquake pairs on the Nankai Trough had lags of either a few days (1–3 August 1361 for the Shohei pair and 23–24 December 1854 for the Ansei pair) or a few years (17 December 1096 to 22 February 1099 for the Kowa/Eicho pair and 7 December 1944 to 21 December 1946 for the Showa pair).

Hyuganada earthquakes

Our model simulated M_w 7.4–7.6 events in the northern part of the Hyuganada segment with recurrence intervals of 81–292 years (Figs. 6; Additional file 1: S3). The time interval between the two Hyuganada events in the historical record (Fig. 1), ~260 years, lies within this range (target phenomenon 2). Aseismic slips, which were also simulated in the asperity area in northern Hyuganada (point 6 in Additional file 1: Fig. S1), would release stress in that area.

Hyodo et al. (2016) showed that whether a great earthquake was triggered by a Hyuganada earthquake depended on the timing of the Hyuganada earthquake. However, because they set a shorter distance between the asperities of Nankai and Hyuganada earthquakes than we did in our model (their Nankai earthquake asperity reached Cape Ashizuri, unlike ours in Fig. 4f), the two asperities in their model could easily influence each other. Although not showing in a figure, when we ran a simulation with a shorter distance between our two asperities (areas including points 4 and 6 in Fig. 4f), it

produced frequently Nankai earthquakes that also ruptured the Hyuganada asperity, a result inconsistent with the historical record. Under the set of spatial parameters necessary to reproduce the historical record, shown in Fig. 4f, no great earthquake initiated at the asperity in northern Hyuganada. Although Hyodo et al. (2016) also suggested that the 1498 Meio Nankai earthquake might have been triggered by a Meio Hyuganada earthquake, both of these earthquakes are doubtful (Ishibashi 1998; Harada et al. 2017). Our results indicate that it is difficult for Hyuganada earthquakes to trigger the Nankai earthquakes. Note that the seismic gap with a recurrence interval of ~260 years may be an apparent one due to the paucity of historical records (see "Slip-deficit rate distribution").

M_w 6-class earthquakes in LSSE areas

In our model, nine *M_w* 6-class earthquakes ruptured the deeper part of the seismogenic zone in segments E and Z (events 17, 21, 28, 42, 43, 46, 50, 63, and 98 in Additional file 1: Fig. S2; green lines in Figs. 6 and Additional file 1: S3). According to the seismic catalog, which includes estimated magnitudes for pre-instrumental events (Usami (2003) for events before 1885, Utsu

(1982) for 1885–1922 events, and Japan Meteorological Agency (2017) for 1923–present events), 7 earthquakes of *M* 6-class occurred in the Tokai district and the Bungo Channel during 1600–2015 (Fig. 8). Although the hypocenter locations of events before 1884 have limited precision, these events might have ruptured the deeper part of the seismogenic zone, similar to the events simulated by our model.

In our simulation, *M_w* 6-class earthquakes or acceleration of slip in the Bungo Channel LSSE area sometimes induced *M_w* ~7.5 Hyuganada earthquakes. For example (see Additional file 1: Fig. S2), *M_w* 6-class earthquakes in the Bungo Channel LSSE area appeared only seven times in 4400 years (events 17, 28, 43, 46, 50, 63, and 98), and for four pairs (events 17–18, 28–29, 46–47, and 50–51) of them, the time differences between the *M_w* 6-class earthquakes and the *M_w* ~7.5 Hyuganada earthquakes were within 0.04 years. In addition, simulated *M_w* ~7.5 Hyuganada earthquakes occurred 31 times in 4400 years, and five (events 22, 54, 66, 77, and 94) of them were earthquakes whose rupture starting point (shown by a star in Additional file 1: Fig. S2) was located in the Bungo Channel LSSE area. In the Tokai LSSE area, in contrast, the slip here did not propagate to the adjacent area and

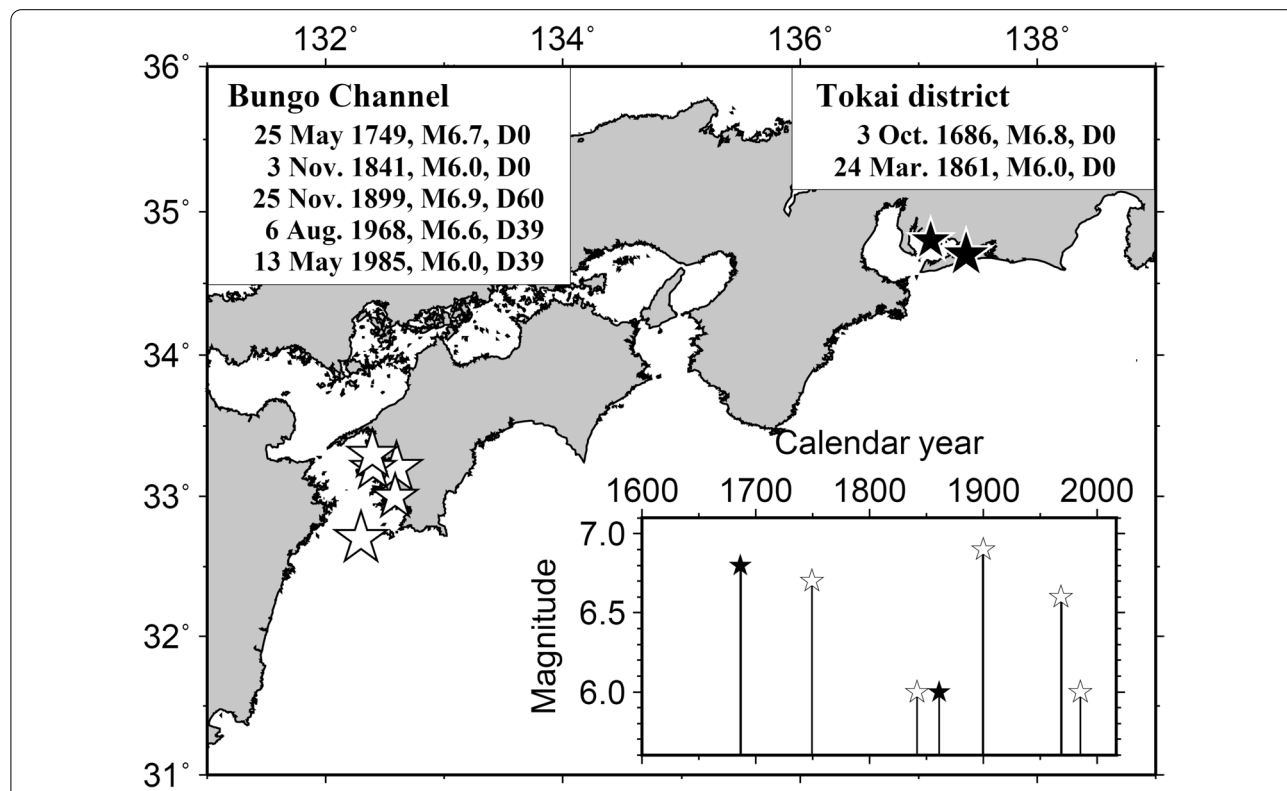


Fig. 8 Epicentral distribution and magnitude diagram of *M* 6-class earthquakes in the Tokai district (solid stars) and the Bungo Channel (open stars) during 1600–2015. D Indicates the depth of an earthquake

M_w 6-class earthquakes (events 21 and 42 in Additional file 1: Fig. S2) in the Tokai LSSE area did not induce any larger event. This is because we modeled subducting ridges by assigning a large σ^{eff} (Sect. "Tuning of effective normal stress σ^{eff} ") and large L (Sect. "Tuning of characteristic displacement L ") to the seismogenic zone (areas including points 1 and 2 in Fig. 4) to suppress the rupture propagation during the 1944 Tonankai earthquake. This modeling also behaved as a barrier against slip in the Tokai LSSE area to propagate into the subducting ridge area, resulting in M_w 6-class earthquakes (events 21 and 42) staying only in the Tokai LSSE area.

In our model, the ruptures of great earthquakes tended to initiate off Cape Shiono (Additional file 1: Figs. S2 and S3). This tendency was an effect not only of the plate configuration (Takayama et al. 2008), but also of the setting of a large L off Cape Shiono in order to reproduce the rupture starting points of the 1944/1946 Showa earthquakes (Additional file 1: Section S2.1) and low slip-deficit rates (Additional file 1: Section S2.4). Because the Tokai and Bungo Channel LSSE areas are far from the initiation points of great earthquakes, there may be no cases of M_w 6-class earthquakes in either of these LSSE areas triggering great earthquakes.

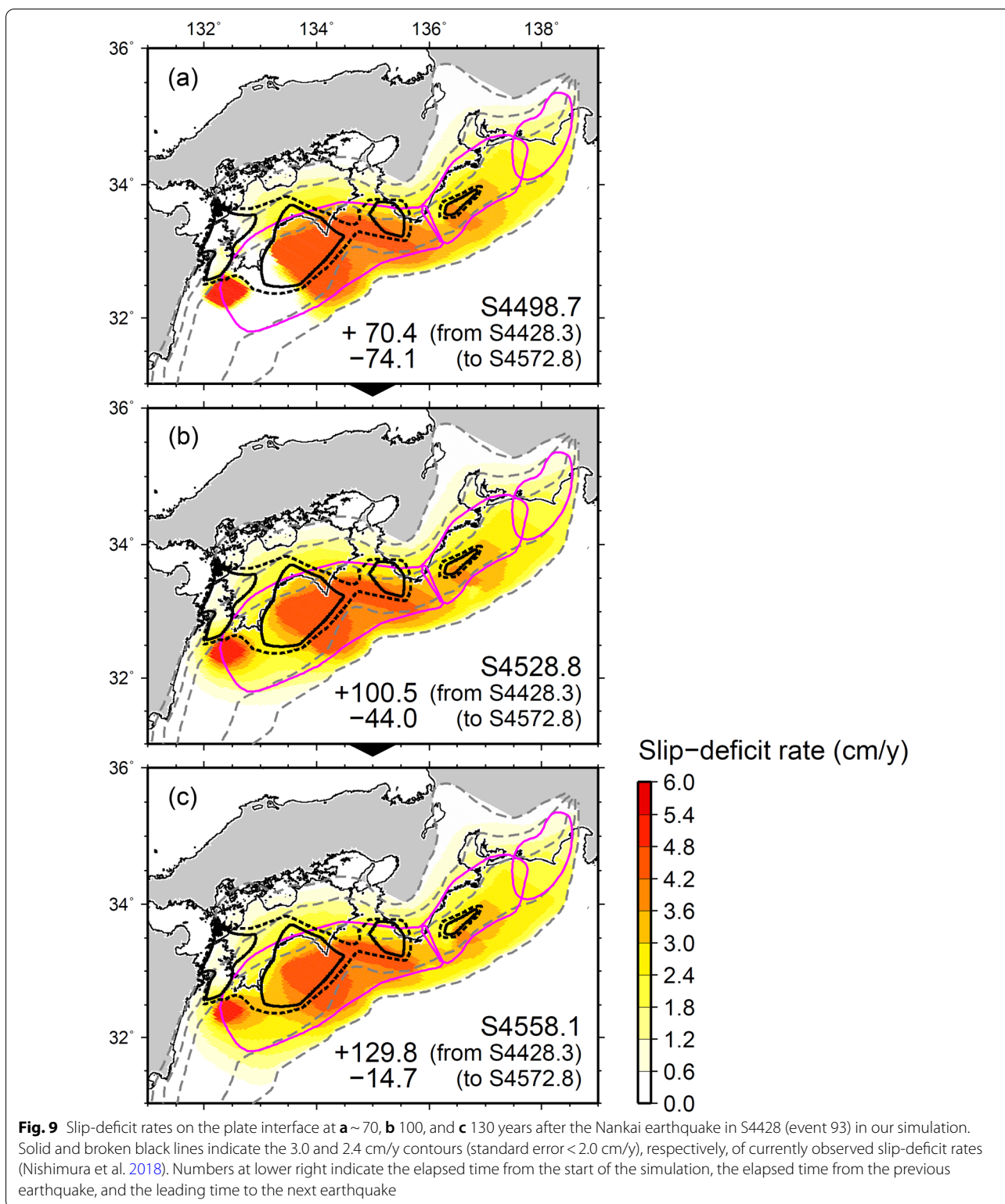
Slip-deficit rate distribution

Offshore observations have recently revealed that slip-deficit rates are heterogeneous on the Nankai Trough plate boundary (Yokota et al. 2016; Nishimura et al. 2018). In this section, we compare slip-deficit rate distributions between our model and observations (Nishimura et al. 2018) (Fig. 2d) by using the sequence of events during S4338–S4491, which is similar to the historical sequence of the 1854 Ansei, 1944/1946 Showa, and 1968 Hyuganada earthquakes. Nishimura et al. (2018) used inland GNSS data from 2005 to 2009 and seafloor GNSS/A data from 2004 to 2016 in a block modeling approach to estimate slip-deficit rates on the plate boundary by superimposing rigid motions between blocks and elastic deformations due to slip defects between blocks. Because more than 70 years have passed since the 1946 Showa Nankai earthquake, we examined the spatial distributions of the slip-deficit rate on the plate interface at ~70, 100, and 130 years after the Nankai earthquake (event 93 at S4428) in our simulation (Fig. 9). The slip-deficit rate is the difference between the plate convergence rate (Fig. 4c) and the slip rate in each cell of the model. In the northern Hyuganada segment, an M_w 7.5 event occurred in S4491, 63 years after event 93, indicating that afterslip around the Hyuganada focal region had temporarily decreased the slip-deficit rate to nearly zero off Cape Ashizuri (Fig. 9a). Then the slip-deficit rate continued to decrease in the Hyuganada focal region while

it recovered slightly in the surrounding area (Fig. 9b, c). Note that the time difference between the Nankai and Hyuganada events in our model (63 years) was longer than that in the historical record (22 years). Although the slip-deficit rate distributions in this example from our model were generally larger than those observed and larger slip-deficit rates extended further up-dip (<10 km depth) than the observation, their spatial patterns were generally similar at all three time points and relatively consistent to the observation.

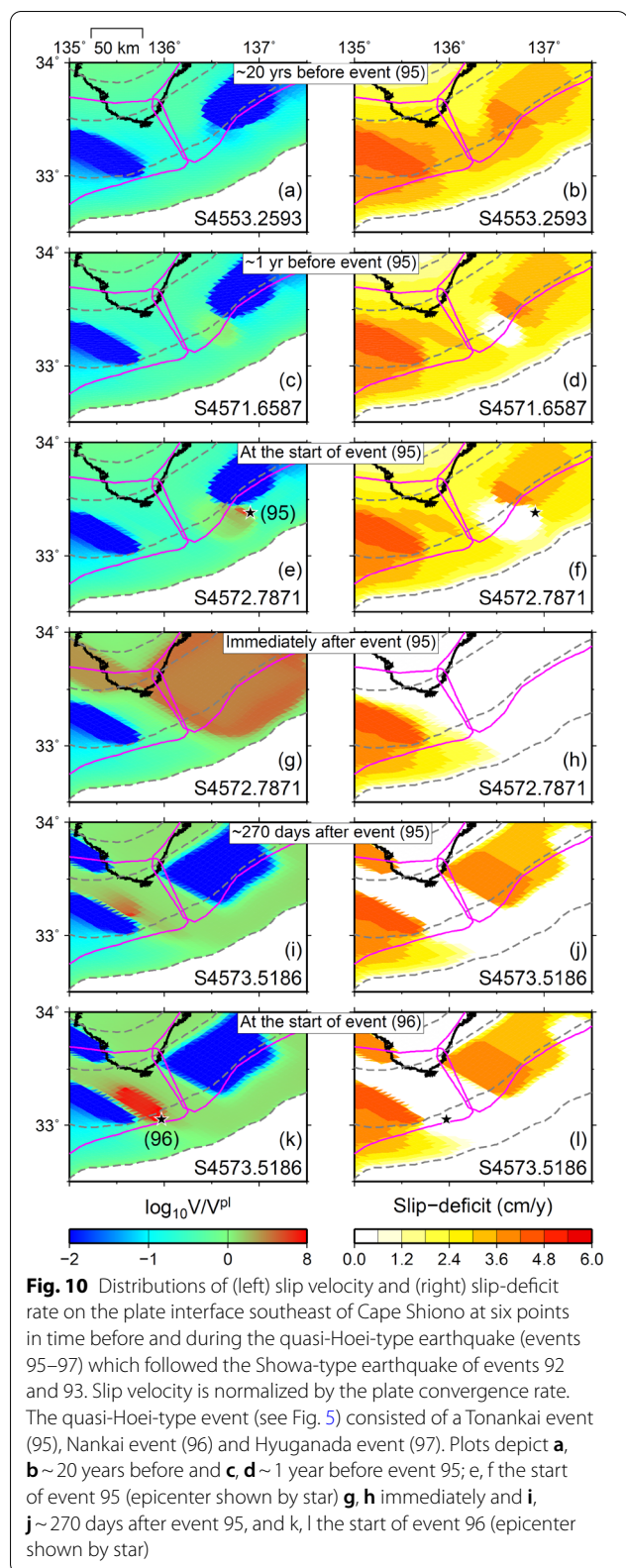
The 4400-year simulation produced several examples of Showa-type event (red outlines in Additional file 1: Fig. S2) that were followed by a great earthquake pair, four that ruptured segments A–D (quasi-Showa type) and one that ruptured segments Z–D (quasi-Hoei type). In these cases, an eastern event of M_w 8.0 and a western event of M_w 8.3 or more occurred with a time lag of about half a year. Figure 10 shows the slip-deficit rate distributions and slip velocity distributions before and after the quasi-Hoei-type earthquake event (events 95–97) that followed a Showa-type event (events 92 and 93). The slip-deficit rates before event 95 in S4572, which ruptured the Tonankai segment, were decreasing slightly, then changed significantly near the starting point, from 3 cm/y to nearly zero off Cape Shiono between S4553 (Fig. 10b) and S4571 (Fig. 10d). After event 95, the interplate coupling in the Tonankai area and the Kii Channel LSSE area recovered, while slip near the starting point of event 96 in S4573, which ruptured the Nankai segment, progressed up-dip and nucleated (see the velocity distribution). The evolution of interplate coupling before and after the quasi-Showa-type events that followed a Showa-type event was similar (for example, events 75–76 and 78–79). The current slip-deficit rate off Cape Shiono is estimated to be almost zero (Nishimura et al. 2018) (Fig. 2d). The high slip-deficit rate region in the Tonankai segment is currently smaller (Fig. 2d) than that in the simulation result for S4572 at the time of event 95 (Fig. 10f), and the next great event has not yet happened. This result suggests that the actual nucleation area may be larger than the area used in our model, with a critical nucleation size of about 27 km (point 3 in Table 2).

Although Nishimura et al. (2018) reported an area of high slip-deficit rate beneath the Bungo Channel, that rate might decrease in the long term because no M_w 7-class LSSE was included in the observation data. When we assigned a large σ^{eff} to northern Hyuganada (point 6 in Fig. 4e) to reproduce the seismic gap of ~260 years, the simulated slip-deficit rate was higher than the observations. Because this difference in slip-deficit rates was large, the apparent absence of earthquakes in the observations may reflect the paucity of the historical record.



Other studies besides Nishimura et al. (2018) have estimated slip-deficit rates on the Nankai Trough plate interface (Noda et al. 2018; Kimura et al. 2019). They reported

slip-deficit rate distributions along the strike direction similar to that of Nishimura et al. (2018). Kimura et al. (2019) also estimated the slip-deficit rate from land-based

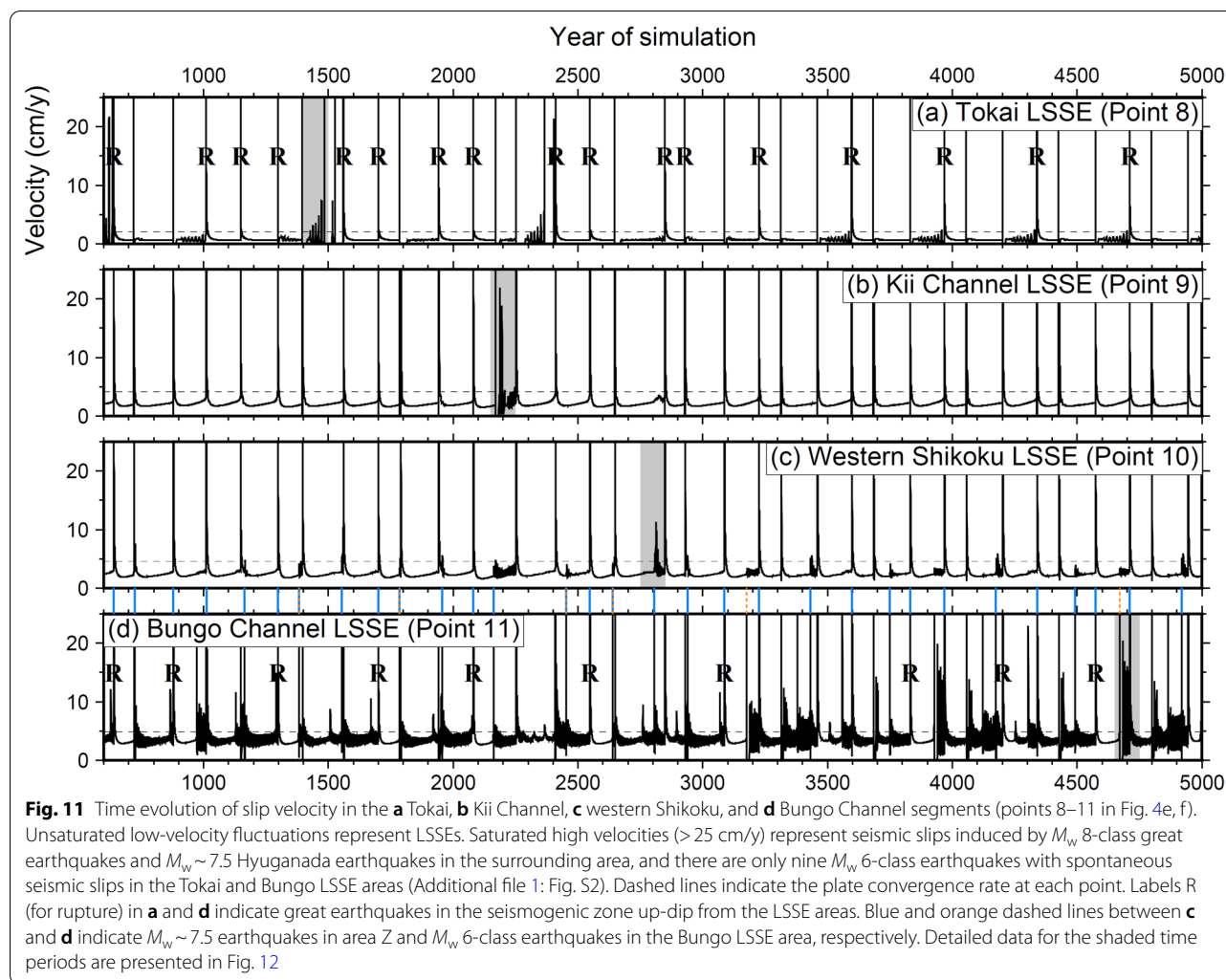


GNSS and seafloor GNSS/A data using a block motion model similar to that of Nishimura et al. (2018), adding observation data from five seafloor GNSS/A stations near Suruga Bay, Kumano Basin, and the trough axis managed by Nagoya University. To make the spatial uncertainty of their estimated values uniform, they included subfaults with low spatial resolution beneath the ocean, reflecting the low spatial density of the seafloor GNSS/A network. This made it possible to estimate slip-deficits near the trough axis, albeit at a lower spatial resolution. High slip-deficit rates were estimated to the south of Cape Ashizuri, the Kii Channel, and the Shima Peninsula. However, these regions have been the site of shallow LSSEs (Yokota and Ishikawa 2020) and VLFs (Takemura et al. 2019), indicating low interplate coupling. In an inversion analysis incorporating viscoelastic response to estimate slip-deficit rates from land-based GNSS and seafloor GNSS/A data, Noda et al. (2018) reported a peak in the slip-deficit rate that was closer to the trough axis than that of Nishimura et al. (2018). Whereas Nishimura et al. (2018) and Kimura et al. (2019) used the same plate configuration model as our study, Noda et al. (2018) used a CAMP model (Hashimoto et al. 2004) that was based mainly on intraplate earthquakes in the Philippine Sea slab. Watanabe et al. (2018) noted that differences in the plate configuration can affect estimates of slip-deficit rates. In sum, we consider the results of Nishimura et al. (2018) to be suitable for comparison with our simulation results.

We confirmed that large L has a certain effect in reproducing low slip-deficit rate distributions, but actual observation results show a much smaller slip-deficit rate southeast of Cape Muroto. To better reproduce the observations, we could set $(a - b)\sigma^{eff}$ close to zero by defining local areas with extremely small σ^{eff} or by making $(a - b)$ positive. Shallow VLFs (Takemura et al. 2019) (Fig. 2d), which indicate the presence of fluid, occur where seamounts and ridges have subducted, indicating locally small σ^{eff} (Fig. 2d). Hori (2006) and Kodaira et al. (2006) assigned $a - b > 0$ to a wedge-shaped area off Cape Shiono to represent the unlocked plate interface based on the existence of the highly fractured oceanic crust caused by strike-slip faults indicating stress release through gradual deformation there. It might be appropriate to do so in other low slip-deficit rate regions if strike-slip faults suggesting the unlocked plate interface are present.

LSSEs

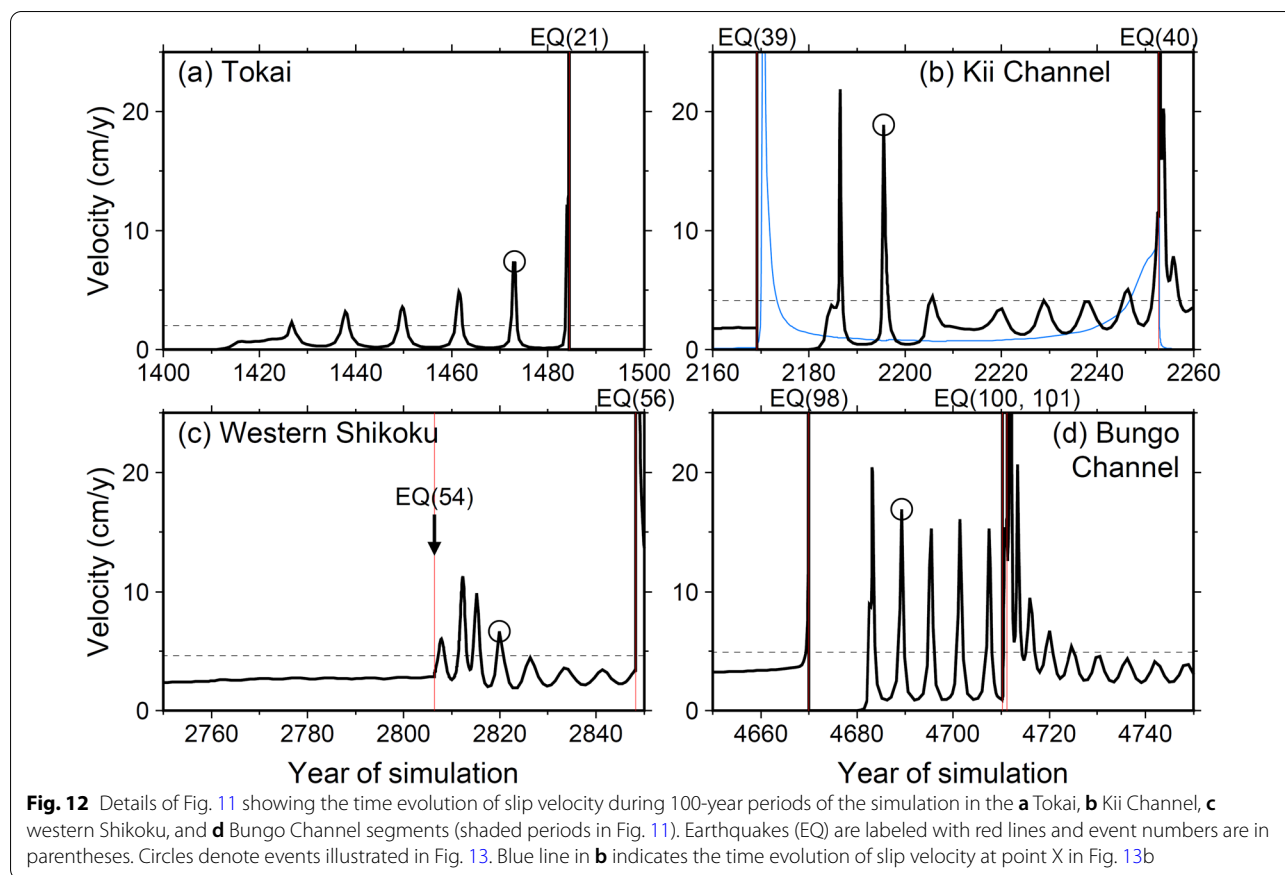
Figure 11 shows four time series of simulated slip velocity in LSSE areas, in which intermediate (unsaturated) peaks



in slip velocity correspond to LSSEs. Beneath the Tokai district (point 8 in Fig. 4e), simulated LSSEs occurred in the latter half of interseismic periods. Beneath the Kii Channel (point 9), the simulated LSSE amplitude was very small, being large only after the unpaired Tonankai earthquake in S2169 (event 39). Beneath western Shikoku (point 10), LSSEs tended to be excited by $M_w \sim 7.5$ earthquakes in northern Hyuganada or $M_w \sim 6$ earthquakes in the Bungo Channel LSSE area. Observations based on GNSS data (Kobayashi 2017; Takagi et al. 2019) indicate the occurrence of western Shikoku LSSEs within one year after Bungo Channel LSSEs. Our simulation appears to reproduce the response of western Shikoku LSSEs to surrounding stress disturbances (although the cause of disturbance is different such as LSSEs in observations and earthquakes in our model). In the Bungo Channel district (point 11), simulated LSSEs were nearly constant throughout the interseismic periods.

Beneath the Tokai and Bungo Channel districts, simulated LSSEs tended not to occur after ruptures up-dip in the seismogenic zone (R in Fig. 11). The stress heterogeneities associated with a non-ruptured seismogenic zone cause LSSEs to be generated in the deeper zone, as pointed out by Hirose and Maeda (2013). In fact, in the Tokai region (segments E and F), the area up-dip of the Tokai LSSE area did not rupture in the 1944 Tonankai earthquake. Likewise, in the Bungo Channel region (segment Z), because the 1946 Nankai earthquake rupture did not extend past Cape Ashizuri, the area up-dip of the Bungo Channel LSSE area did not rupture.

Figure 12 shows detailed time series of simulated LSSEs in the 100-year periods shown shaded in Fig. 11. The recurrence interval of the simulated Tokai LSSEs was 11.3–11.8 years, and their amplitudes increased with time until the M_w 6-class earthquake (event 21) in S1484.



The recurrence interval of the simulated Kii Channel LSSEs was 8.8–14.4 years, and their amplitudes varied. Prior to event 40, the slip accelerated at the lower end of the Nankai asperity (blue line in Fig. 12b), the pre-slip progressed to the shallow plate interface, and the rupture started near the trough axis (Additional file 1: Fig. S2). The increase in LSSE amplitude several years before event 40 was due to the pre-slip at the lower end of the asperity, and it is unlikely that it directly triggered event 40. The recurrence interval of the simulated western Shikoku LSSEs was 2.9–7.7 years, and their intervals lengthened and their amplitudes decreased with time. The simulated Bungo Channel LSSEs differed before and after the S4711 Hyuganada earthquake (event 101). Before the earthquake, the variations of the recurrence interval (6.0–6.1 years) and the amplitude were small, and afterward the amplitude first became large and then decreased with time, whereas the occurrence interval was initially short and then increased with time.

Because Bungo Channel LSSEs before 1980 could not be estimated, even with pre-GNSS geodetic data (Kobayashi and Yamamoto 2011), we could not confirm velocity changes of the western Shikoku and Bungo Channel LSSEs before and after the 1968 Hyuganada earthquake.

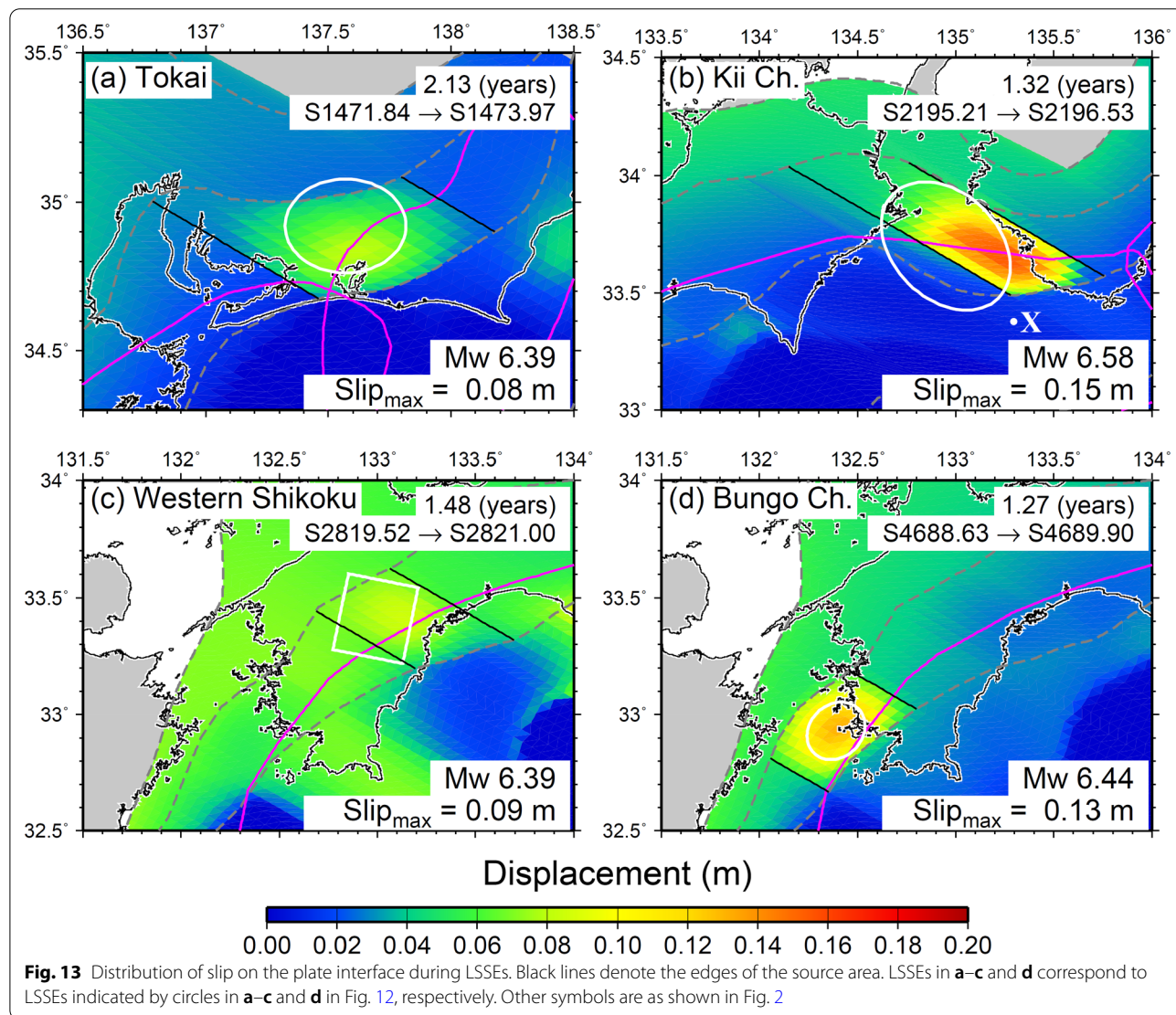
In general, the occurrence intervals of the simulated LSSEs were consistent with the observations (Ozawa 2017). Note that the simulated LSSEs did not directly trigger great Nankai earthquakes, because they were too distant from the earthquake epicenters.

The critical nucleation size h^* in the Tokai LSSE area (point 8) is slightly smaller than those in the other LSSE areas (Table 2). Since the ratio of the asperity size to the critical nucleation size is large, unstable sliding is likely to occur (Kato 2003). As a result, Tokai LSSEs may have tended to increase gradually in amplitude, and in some cases seismic slip may have occurred (Fig. 12a). The recurrence interval of earthquakes is roughly regulated by $(b - a)\sigma^{\text{eff}}$ of the seismogenic zone (e.g., Stuart 1988) and the plate convergence rate (e.g., Hirose and Maeda 2013). Because the plate convergence rate is slower in the east than in the west (Nishimura et al. 2018) (Fig. 4c), recurrence intervals should be longer in the east if the friction parameters are the same. Comparing the three segments other than Tokai, which have the same friction parameters (Fig. 12), it can be confirmed that the recurrence interval is slightly longer in the Kii Channel, in the east. The nucleation size also depends on the aspect ratio of a rectangular asperity, and when the ratio $\alpha = w/l$,

where w and l indicate the fault width and length, is large, the nucleation size becomes small (Kato 2003). Although it is a qualitative consideration, because the shape of the LSSE area is not a simple rectangle, the Kii Channel LSSE area (point 9) should tend more toward unstable sliding than the Bungo Channel LSSE area (point 11), yet the seismic slip occurred in the Bungo Channel. Differences in the nucleation size of the LSSE area may not be the only defining characteristics of LSSEs, because all LSSEs tend to end with a transition to stable sliding at the plate convergence speed and because LSSEs are excited by ambient stress heterogeneity and disturbances. These differences also probably affect the LSSE velocity and recurrence interval in each area.

Figure 13 shows the spatial distributions of slips on the plate interface during the LSSEs marked with circles

in Fig. 12. We estimated LSSE magnitudes within areas with small σ^{eff} and L (Fig. 4e, f) by summing over the period when the slip rate exceeds the plate convergence rate at the reference points for those areas (points 8–11). The magnitudes of the simulated LSSEs in the Kii Channel and western Shikoku segments were consistent with the observations (see Fig. 6 in Ozawa 2017), but those in the Tokai and Bungo Channel segments were underestimated compared to the observations. Hirose and Maeda (2013) showed that large values of $(b - a)\sigma^{\text{eff}}$ or small L values lead to LSSEs with large magnitudes. However, large values of $(b - a)\sigma^{\text{eff}}$ are inappropriate because they also lengthen the recurrence interval of LSSEs and are inconsistent with the observation. In our model, although LSSE amplitude increased as L decreased, the calculations tended to become unstable as L approached the size



of the computation cells (see "[Computational instability due to cell size](#)"). Therefore, L cannot be reduced any further given the resolution of our model. Because the calculation cost increases with the resolution of the model, reproducing the magnitudes of LSSEs in these areas must await future studies. Ochi and Kato (2013), who did not eliminate steady-state fluctuations associated with plate subduction, have suggested that the moment magnitude of the 2000–2005 Tokai LSSE was 6.6, not 7.2; in that case, the simulated Tokai LSSE would be consistent with observations. Because we estimated LSSE magnitudes simply from the amount of slip during the period, it is appropriate to compare our results with those of Ochi and Kato (2013). Note that the magnitude of Bungo Channel LSSEs is the same with or without steady-state fluctuations (Ochi 2015). The durations of simulated LSSEs were about 1–2 years in all areas (Fig. 13), shorter

than the observed durations (Fig. 3) except in the Bungo Channel segment.

Figure 14 plots the evolving relationship between the slip velocity and the shear stress during various events in the four LSSE areas. In the Tokai LSSE area (Fig. 14a), when the area up-dip of the Tokai LSSEs did not rupture during event 19 (note that the curve begins just before event 19), the shear stress was almost constant as the velocity dropped sharply and the plate interface stuck firmly once. After that, LSSEs occasionally released the accumulated stress, as shown by the tight loops in the curve. On the other hand, after event 13, which ruptured the area up-dip from the LSSE area, the shear stress increased as the velocity decreased and then stagnated near the plate convergence rate, and stress was released through stable sliding, such that LSSEs did not occur.

In the Kii Channel segment (Fig. 14b), the behavior after the isolated Tonankai earthquake (event 39) was

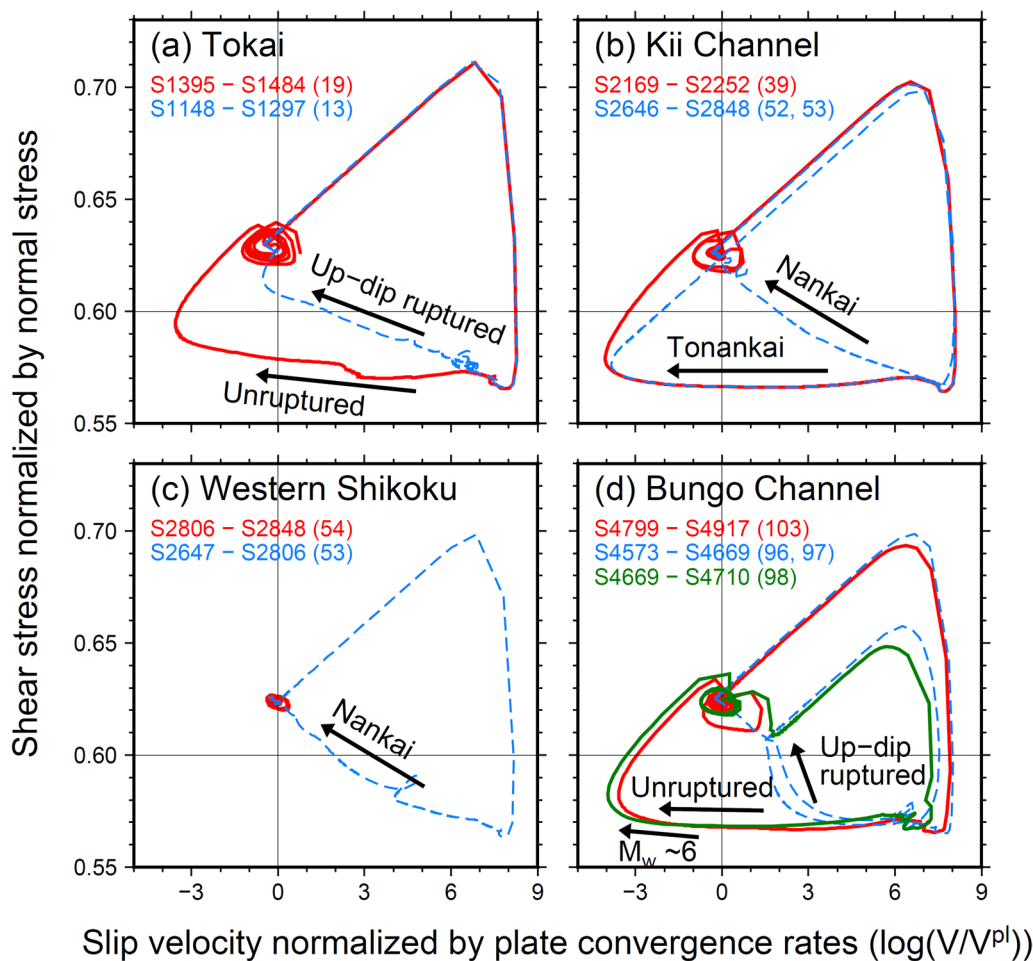


Fig. 14 Trajectory diagrams showing the relation between slip velocity and shear stress in the **a** Tokai, **b** Kii Channel, **c** western Shikoku, and **d** Bungo Channel segments (points 8–11 in Fig. 4e, f). Each line corresponds to the simulation period shown at upper left and includes the number of the event during that period, shown in Additional file 1: Fig. S2

similar to the case in which LSSEs occurred in the Tokai LSSE area. Under the influence of the adjacent Nankai asperity (point 4) up-dip from the Kii Channel LSSE area, which did not rupture, the Kii Channel LSSE area stuck firmly once, and then stress was released by occasional LSSEs. On the other hand, in a case of sequential rupture of the Tonankai and Nankai segments (events 52 and 53), after the Tonankai earthquake (event 52), the shear stress remained almost constant as the velocity dropped sharply and the plate interface stuck firmly once, as in the case of event 39. However, the Nankai earthquake (event 53) soon followed, and then the velocity stagnated near the plate convergence rate and stress was released by stable sliding, such that LSSEs did not occur.

In the western Shikoku segment (Fig. 14c), after the Nankai earthquake (event 53), the velocity stagnated near the plate convergence rate and entered a stable sliding cycle (see Figs. 11, 12). This is the reason why the Nankai asperity (point 4) up-dip from the LSSE area ruptured during every Nankai earthquake (the timing of the large slip velocity > 25 cm/y in Fig. 11c is the same as the rupture of the Nankai asperity). However, LSSEs occurred as a result of the stress disturbance caused by an $M_w \sim 7.5$ earthquake in northern Hyuganada (blue lines in Fig. 11c or event 54 in Fig. 12c) or an $M_w \sim 6$ earthquake in the Bungo Channel LSSE area (orange dashed lines in Fig. 11c). Their amplitude tended to decrease with time.

In the Bungo Channel segment (Fig. 14d), as in the Tokai LSSE area, LSSEs occasionally occurred when the area up-dip was unruptured (event 103) and did not occur when it was ruptured (events 96 and 97). After an $M_w \sim 6$ earthquake in the Bungo Channel LSSE area (event 98), the behavior was the same as when the up-dip area was unruptured. That is, the potential for LSSEs was increased by the combination of an unruptured up-dip area, as in the Tokai LSSE area (Fig. 14a), and the stress disturbance from middle-class earthquakes, as in the western Shikoku LSSE area (Fig. 14c). Observations (Fig. 3) show that LSSE activity is greater in the Bungo Channel than in other LSSE areas. From the above, our simulation shows that LSSEs are excited by heterogeneity and disturbances in ambient stress, and that it is important that the plate interface sticks firmly once under the conditionally unstable state (where $a - b < 0$ and the LSSE area size is comparable to h^*).

Among simulated LSSEs beneath the Kii Channel (point 9), only the set of LSSEs after the S2169 unpaired Tonankai earthquake was large, which was caused by a heterogeneous stress distribution due to an unruptured up-dip area (adjacent Nankai asperity) like Tokai and Bungo Channel LSSEs. However, in fact the 1946 Nankai earthquake ruptured the area up-dip from the LSSE area (Baba and Cummins 2005; Murotani et al. 2015)

(Fig. 2a) and LSSEs have occurred beneath the Kii Channel at least since 1996 (e.g., Kobayashi 2014, 2017; Ozawa 2017). Accordingly, our model did not simulate them. Although we cannot clarify the reason for this at present, one possible explanation is that an unknown heterogeneous stress distribution was generated beneath the Kii Channel at the 1946 Nankai earthquake.

The configuration of the Philippine Sea slab varies greatly. Mitsui and Hirahara (2006), modeling the effect of slab dip angle on LSSE occurrence, pointed out that lateral changes of slab dip are important factors controlling LSSE occurrence. After that, however, the increase in knowledge of plate configuration and LSSEs reveals that LSSEs also occur in areas where dip changes in the strike direction of the slab are small, such as western Shikoku and Bungo Channel (Fig. 4e, f). Consequently, lateral changes of slab dip are a factor affecting LSSE distributions, but not a necessary condition for LSSEs.

With regard to the relationship between the slab configuration and fluid distributions, Morishige and van Keken (2017) showed in a 3-D fluid model that fluids released from the slab are localized depending on the slab configuration, and they suggested that fluids beneath the Kii Channel tend to migrate away. Seismic tomography results (see cross section in Fig. 6 of Hirose et al. 2008) indicate that there is less fluid beneath the Kii Channel than beneath the Tokai district and the Bungo Channel. In this study, we assigned the same effective normal stress σ^{eff} to the Kii Channel, western Shikoku, and Bungo Channel LSSE areas, but it may be that the Kii Channel should have a larger σ^{eff} value. However, since σ^{eff} defines the LSSE recurrence interval (Hirose and Maeda 2013), it is constrained by the observed values (Fig. 3) to a limited range of variation.

Although LSSE areas occur in a consistent depth range, $(b - a)\sigma^{\text{eff}}$ must change greatly along the trough axis because LSSE areas are intermittent along the axis. Because frictional parameters a and b depend on depth (Blanpied et al. 1998), $(b - a)$ should vary little along the trough axis; accordingly, it would be appropriate to allow σ^{eff} to be heterogeneous, as in this study. However, it has been pointed out that $(a - b)$ also depends on σ^{eff} (Sawai et al. 2016) and sliding velocity (Boulton et al. 2018). Therefore, both σ^{eff} and $(b - a)$ would change along the trough axis with variations in fluid presence, even if the depth of the LSSE zone is constant. To produce more realistic models, parameters will need to be chosen with this in mind.

Problems to address in future studies

It is well known that a non-planar fault induces changes in normal stress that can significantly alter the fault strength under both static and dynamic loading (e.g.,

Dieterich and Smith 2009). In addition, Linker and Dieterich (1992) described RSF with a different state evolution law for normal stress changes. In this study, the triangular cells were arranged to fit the configuration of the plate boundary, but we did not consider the temporal variation of normal stress for the following reasons. Takayama et al. (2008) showed that, owing to shear slip, the value of the slip response function is 1–3 orders of magnitude smaller in the normal direction than the shear direction for the same 3-D plate configuration used in this study. That is, the temporal variation of normal stress due to shear slip is small compared to that of shear stress. Moreover, incorporating the temporal variation of normal stress doubles the calculation cost, which is not realistic for parameter tuning by trial and error, as we did in this study. Note that previous studies have not considered the temporal variation of the normal stress in simulations that introduced 3-D plate configurations in the Nankai Trough (Hirose and Maeda 2013; Hyodo and Hori 2013; Nakata et al. 2014; Hyodo et al. 2016). This remains an issue for future work.

The quasi-dynamic simulation used in this study approximates the stress change associated with the radiation of seismic waves by the effect of the radiation damping term (the second term on the right side of Eq. (1)). On the other hand, fully dynamic simulations fully incorporate stress changes associated with the propagation of seismic waves (e.g., Lapusta et al. 2000; Kaneko et al. 2010). Since fully dynamic simulation is computationally very expensive (Thomas et al. 2014), it is not realistic to apply it to a 3-D model of the entire Nankai Trough. Thomas et al. (2014) reported that fully and quasi-dynamic simulations generated similar slip patterns, although the slip velocity, the rupture propagation speed, and the degree of rupture stopping in the velocity-strengthening region during an earthquake were quantitatively different. Lapusta and Liu (2009) showed that a quasi-dynamic simulation set to the seismic radiation correction factor $\eta = 4$ in Eq. (1) had high similarity to a fully dynamic simulation, but differed from it in detail with respect to the slip velocity, rupture propagation speed, and slip amount during an earthquake; they also found that the rupture pattern in the quasi-dynamic simulation appeared monotonous compared to that in the fully dynamic simulation. In this study, we set $\eta = 1$ according to previous studies (e.g., Hori 2006; Hyodo and Hori 2013; Hirose and Maeda 2013; Nakata et al. 2014; Hyodo et al. 2016). When rescaled with η , the behaviors of $\eta = 1$ and $\eta = 4$ during an earthquake match well (Lapusta and Liu 2009). Therefore, even if $\eta = 4$ is set in this study, the rupture pattern will not change significantly qualitatively. Note that a quasi-dynamic simulation

with $\eta = 3$ was performed off Tohoku by Nakata et al. (2016).

There is growing evidence that friction may be much lower at seismic slip velocities than RSF laws predict (e.g., Di Toro et al. 2004; Rice 2006). When this seismic weakening mechanism was introduced into the friction constitutive law, the behavior was significantly different between fully and quasi-dynamic simulations, and the rupture pattern became more complicated in the latter (Thomas et al. 2014). In the case of a simple two-dimensional model where two velocity-weakening regions were embedded in the velocity-strengthening region, earthquakes that ruptured both of them at once were repeated in a fully dynamic simulation, whereas small earthquakes that ruptured part of one velocity-weakening region were frequent in the quasi-dynamic simulation while large earthquakes that ruptured the entire area were rare. Accordingly, if we had incorporated a seismic weakening mechanism in our quasi-dynamic simulation, even if we had assigned the same parameters to the regions including points 1–3 and points 4–5 in Fig. 4f, we might have been able to reproduce the complex rupture patterns shown in Fig. 1. On the other hand, because a fully dynamic model with a seismic weakening mechanism produces a very simplified rupture pattern, parameter distributions must be more complicated than what we used to reproduce these rupture patterns. This is a future issue.

We targeted rupture areas (Fig. 1) on the basis of the Earthquake Research Committee (2013) compilation, but different interpretations are possible. Seno (2012) proposed a model in which Ansei- and Hoei-type earthquakes alternate, Ansei-type earthquakes rupturing segments A, B, and D–F (Fig. 1) at intervals of 356–412 years, and Hoei-type earthquakes rupturing segments A–D at intervals of 237–474 years. According to that model, the next great Nankai Trough earthquake would not occur for another 200 years. The Hoei-type earthquake of Seno (2012) corresponds to our Showa-type and quasi-Showa-type earthquakes, which were common in our simulation; however, our simulation did not produce any of Seno's Ansei-type earthquakes because it was not one of our targeted phenomena. To do so, our model might have to allow effective normal stress to vary with time, as Seno (2012) suggested.

In our model, the eastern edges of Tokai/Tonankai earthquake ruptures did not vary much after S3000 (Additional file 1: Fig. S3), a result suggesting that this pattern may constitute a limit cycle. In addition, except for the Nankai earthquakes of events 88 and 96, the sequence of quasi-Showa-, Ansei-, and Showa-type events occurred repeatedly. This condition might be fundamental to actual great earthquakes along the

Nankai Trough. By adding perturbations representing phenomena that we did not incorporate previously, our model might reproduce, more complicated and realistic phenomena. For instance, SSSEs of M_w 5–6 have also occurred at the edge of the seismogenic zone (Nishimura et al. 2013), and the interaction with great earthquakes is a concern. An M_w 5.8 earthquake on 1 April 2016 appeared to occur on the plate boundary off Cape Shiono. Because this location is near the starting point of the 1944 Showa Tonankai earthquake, an M_w 6-class asperity should be included in the future simulations with our model. In addition, Pollitz and Sacks (1995) estimated that the M_w 8.0 1891 Nobi earthquake in the continental plate beneath central Japan has delayed the anticipated Tokai earthquake by at least 20 years. Incorporating stress perturbations associated with surrounding earthquakes (e.g., Kuroki et al. 2004) would make our simulation model more realistic.

As discussed in “Plate configuration” section, we had to modify the near-surface domain of our model because the upper end of the plate boundary in the Nankai Trough axis is at a water depth of 4–5 km. In an alternative model incorporating the effect of surface topography, the large calculation errors in very shallow regions are partially obviated by assigning positive $a - b$ values, which produce steady slip, to those regions (Ohtani and Hirahara 2015). However, analysis of a core sample collected off Cape Shiono has shown that coseismic slip propagated to the trough axis at least once (Sakaguchi et al. 2011). Therefore, it is necessary to assign negative $a - b$ to the trough axis, as we did, and errors in shallow cells would therefore affect the slip behavior. Although setting a smaller cell size would improve the model accuracy, it would also increase computational costs. Consequently, our model did not incorporate surface topography.

It has been pointed out that the configuration of the eastern end of the Philippine Sea plate, east of 138°E and north of 35°N in the Tokai region, is shallower than that used in this study (Matsubara et al. 2021). Although differences in plate configuration are known to affect simulation results (e.g., Takayama et al. 2008), the relatively low plate convergence rate in this region (Fig. 4c) means the effect on our results should be small.

We modeled general aspects of historical earthquakes, including seismic and aseismic slips, to some extent by applying constant a and $a - b$ and heterogeneous σ^{eff} and L to the model space, and presented the best model for reproducing the historical events. Different results can be obtained by using other parameter distributions (see Additional file 1: Section S2). For example, when we changed L from the best model value of 0.22 m to 0.25 m (a change in critical nucleation size from 62.9 km

to 71.4 km) at point 2 off the Tokai district, variation was suppressed at the eastern edge of simulated Tokai/Tonankai earthquake ruptures. As another example, even the small change of making the parameters of the LSSE areas beneath the Kii Channel and western Shikoku the same as those in the surrounding areas affected the simulated earthquake record. Thus, the precise simulation of recurring LSSEs beneath all of southwestern Japan, including Kyushu, is essential to improve models of great earthquakes. This in turn requires improvements in the monitoring technology for LSSEs.

In this study, we focused on reproducing various phenomena on the Nankai Trough plate boundary. However, most geodetic stations are on land, and it remains necessary to verify whether stations on land can capture changes of state at any location on the plate boundary. In addition, it is essential to construct a simulation model that can simulate various phenomena comprehensively, including crustal deformation, before it will be possible to attempt precise forecasts of the next great Nankai earthquake.

Although many offshore seismic stations have been emplaced in recent years, the spatial density of offshore stations is much lower than that of inland stations. A high-density network similar to DONET (Kaneda et al. 2015; Kawaguchi et al. 2015) on the seafloor of the Nankai Trough would be very useful for monitoring earthquakes, tsunamis, and crustal deformation in real time. Denser station coverage on the seafloor will improve the resolution of interplate coupling estimates, which will lead to more realistic models of the Nankai Trough plate boundary.

Conclusions

In this study, we tried to reproduce numerically various phenomena on the Nankai Trough plate boundary and to clarify the characteristics of the parameters that affect each phenomenon. Our best model yielded a 4400-year record of simulated great earthquakes with spatiotemporal diversity. We successfully modeled the along-strike extent of rupture areas and, to an extent, the recurrence intervals of the three most recent event sets of historical events. Our model's estimate of the time lag between the Showa Tonankai and Nankai earthquakes and the recurrence interval of mega-earthquakes, such as the 1707 Hiei earthquake, was consistent with observations. We also successfully modeled the general slip distributions of the relatively well-known Showa Tonankai and Nankai earthquakes. Although our simulated slip-deficit rates tended to be larger than observations, their heterogeneous distributions were relatively consistent with observations. Our model was able to reproduce the occurrence interval of M_w 7.5 events in the northern part of

Hyuganada of ~260 years. It produced no cases in which a Hyuganada earthquake triggered a Nankai earthquake. We found it necessary to apply a small effective normal stress to the Hyuganada asperity to reproduce precisely the slip-deficit rate distribution in northern Hyuganada, but that step shortened the recurrence interval of Hyuganada earthquakes, which suggests the seismic gap in the historical record instead may be an artifact of the sparsity of earthquakes due to the lack of historical documents. In general, the occurrence intervals of simulated LSSEs in the deeper part of the plate boundary beneath the Tokai district, the Kii Channel, western Shikoku, and the Bungo Channel were consistent with observations. All LSSEs tended to end in a gradual transition to in a stable sliding at the plate convergence speed, and LSSEs were excited by heterogeneity and disturbances in ambient stress.

Our 4400-year model simulation showed that Tokai/Tonankai events and Nankai events typically occurred in pairs separated by less than 3 years, but they sometimes occurred simultaneously, and unpaired Tonankai earthquakes were rare. The rupture areas of these paired events varied greatly, and the maximum displacement and the magnitude differed among paired events even when the rupture area were the same. In addition, the simulated record showed that the next great earthquake following a Showa-type event ruptured segments A–D or Z–D and consisted of an eastern event with M_w 8.0 and a western event with M_w 8.3 or more, separated by half a year.

The Tonankai asperity, where ruptures tended to initiate first, followed neither a time-predictable model nor a slip-predictable model. However, the slip-predictable model fit asperities that tended to slip in association with the rupture of an adjacent asperity (points 2, 4, and 5). This finding may be important for evaluating the occurrence potential of the next great earthquake on a Nankai Trough segment.

The results of our simulations depend on the choice of various parameter values and frictional constitutive laws. To further improve the model, it would be desirable not only to incorporate M_w 6-class asperities, occurrence patterns of SSSEs and stress perturbations of the surrounding seismicity into the model, but also to strengthen seafloor observatory networks to better monitor offshore phenomena and the coupling state on the plate boundary.

Abbreviations

3-D: Three-dimensional; GNSS: Global Navigation Satellite System; GNSS/A: GNSS-Acoustic; LSSE: Long-term slow slip event; M_w : Moment magnitude; RSF: Rate- and state-dependent friction; SSSE: Short-term slow slip event; VLFE: Very low frequency event.

Supplementary Information

The online version contains supplementary material available at <https://doi.org/10.1186/s40623-022-01689-0>.

Additional file 1. The occurrence history of all earthquakes in our best model and details of the parameter tuning to obtain the bestmodel.

Acknowledgements

We thank ITO Hidemi for use of his simulation program. We thank Dr. HOSAKA Masahiro for his cooperation in speeding up the calculation code. We also thank Dr. NISHIMURA Takuya for providing the slip-deficit rate and plate convergence rate data. This manuscript was greatly improved by careful reviews of Dr. HIRAHARA Kazuro and an anonymous reviewer. Figure 2e uses gravity anomaly data from the International Gravimetric Bureau. Isodepth contour data were provided by the Meteorological Research Institute. Figures were drawn with GMT (Wessel et al. 2013).

Author contributions

HF conducted simulation runs, analyzed data, wrote most of the manuscript, and made the figures and tables. MK offered suggestions about the organization of the manuscript and helped with the preparation of the manuscript. FK helped with the preparation of the manuscript. KA offered suggestions about the organization of the manuscript and helped with the preparation of the manuscript. All authors read and approved the final manuscript.

Funding

This research was conducted with support from the Japan Meteorological Agency.

Availability of data and materials

Gravity anomaly data are available from the website of the International Gravimetric Bureau (<http://bgi.obs-mip.fr/data-products/grids-and-models/wgm2012-global-model/>). Isodepth contour data are available from the website of the Meteorological Research Institute (<https://www.mri-jma.go.jp/Dep/sei/fhirose/plate/en.PlateData.html>).

Declarations

Ethics approval and consent to participate

Not applicable.

Consent for publication

Not applicable.

Competing interests

The authors have no competing interests.

Author details

¹Meteorological Research Institute, Japan Meteorological Agency, 1-1 Nagamine, Tsukuba, Ibaraki 305-0052, Japan. ²Seismology and Volcanology Department, Japan Meteorological Agency, 3-6-9 Toranomon, Minato-ku, Tokyo 105-8431, Japan.

Received: 31 January 2022 Accepted: 10 August 2022

Published online: 24 August 2022

References

- Aida I (1981a) Numerical experiments of historical tsunamis generated off the coast of the Tokaido district (in Japanese with English abstract). *Bull Earthq Res Inst* 56:367–390
- Aida I (1981b) Numerical experiments for the tsunamis generated off the coast of the Nankaido district (in Japanese with English abstract). *Bull Earthq Res Inst* 56:713–730
- Baba T, Cummins PR (2005) Contiguous rupture areas of two Nankai Trough earthquakes revealed by high-resolution tsunami waveform inversion. *Geophys Res Lett* 32:L08305. <https://doi.org/10.1029/2004GL022320>

- Blanpied ML, Marone CJ, Lockner DA, Byerlee JD, King DP (1998) Quantitative measure of the variation in fault rheology due to fluid-rock interactions. *J Geophys Res* 103:9691–9712. <https://doi.org/10.1029/98JB00162>
- Boulton C, Barth NC, Moore DE, Lockner DA, Townend J, Faulkner DR (2018) Frictional properties and 3-D stress analysis of the southern Alpine Fault, New Zealand. *J Struct Geol* 114:43–54. <https://doi.org/10.1016/j.jsg.2018.06.003>
- Central Disaster Management Council (2001) Report of the specialized investigation committee about Tokai earthquake (in Japanese). <http://www.bousai.go.jp/jishin/tokai/senmon/pdf/siryoku2-2.pdf>, (2021-09-01)
- Di Toro G, Goldsby DL, Tullis TE (2004) Friction falls towards zero in quartz rock as slip velocity approaches seismic rates. *Nature* 427:436–439. <https://doi.org/10.1038/nature02249>
- Dieterich JH (1979) Modeling of rock friction. *J Geophys Res* 84:2161–2175. <https://doi.org/10.1029/JB084iB05p02161>, <https://doi.org/10.1029/JB084iB05p02169>
- Dieterich JH (1981) Constitutive properties of faults with simulated gouge. *Mechanical Behavior of Crustal Rocks*. *Geophys Monogr* 24:103–120. <https://doi.org/10.1029/GM024p0103>
- Dieterich JH (1992) Earthquake nucleation on faults with rate- and state-dependent strength. *Tectonophysics* 211:115–134. [https://doi.org/10.1016/0040-1951\(92\)90055-B](https://doi.org/10.1016/0040-1951(92)90055-B)
- Dieterich JH, Smith DE (2009) Nonplanar faults: mechanics of slip and off-fault damage. *Pure Appl Geophys* 166:1799–1815. <https://doi.org/10.1007/s00024-009-0517-y>
- Earthquake Research Committee (2001) Long-term evaluation of earthquakes in the Nankai trough (in Japanese). http://www.jishin.go.jp/main/chousa/kaikou_pdf/nankai.pdf, (2021-09-01)
- Earthquake Research Committee (2013) Long-term evaluation of earthquakes in the Nankai trough, 2nd ed. (in Japanese). http://www.jishin.go.jp/main/chousa/kaikou_pdf/nankai_2.pdf, (2021-09-01)
- Fujita K, Hirose F, Maeda K (2018) Simulation of recurring earthquakes along the Japan trench (in Japanese). Fall meeting of Seismological Society of Japan S08–P09
- Furumura T, Imai K, Maeda T (2011) A revised tsunami source model for the 1707 Hōei earthquake and simulation of tsunami inundation of Ryujin Lake, Kyushu, Japan. *J Geophys Res* 116:B02308. <https://doi.org/10.1029/2010JB007918>
- Geospatial Information Authority of Japan (2015) Crustal movements in the Chugoku and Shikoku districts (in Japanese). Proceeding of the Coordinating Committee for Earthquake Prediction, Japan 93:336–343. https://cais.gsi.go.jp/YOCHIREN/report/kaihou93/09_03.pdf
- Guatteri M, Spudich P, Beroza GC (2001) Inferring rate and state friction parameters from a rupture model of the 1995 Hyogo-ken Nanbu (Kobe) Japan earthquake. *J Geophys Res* 106:26511–26521. <https://doi.org/10.1029/2001JB000294>
- Hacker BR, Abers GA, Peacock SM (2003) Subduction factory 1. Theoretical mineralogy, densities, seismic wave speeds, and H₂O contents. *J Geophys Res* 108(B1):2029. <https://doi.org/10.1029/2001JB001127>
- Harada T, Nishiyama A, Satake K, Furumura T (2017) The Hyuga-nada Earthquake on June 30th, 1498 is a fake earthquake: examination of the damage descriptions in the war chronicle Kyushu-gunki (in Japanese with English abstract). *J Seism Soc Jpn* 2(70):89–107. <https://doi.org/10.4294/zisin.2016-13>
- Hashimoto M (2022) Is the long-term probability of the occurrence of large earthquakes along the Nankai Trough inflated?—Scientific Review. *Seismol Res Lett* 93(4):2311–2319. <https://doi.org/10.1785/0220210152>
- Hashimoto C, Fukui K, Matsuura M (2004) 3-D modelling of plate interfaces and numerical simulation of long-term crustal deformation in and around Japan. *Pure Appl Geophys* 161:2053–2068. <https://doi.org/10.1007/s00024-004-2548-8>
- Hirose T, Bystricky M (2007) Extreme dynamic weakening of faults during dehydration by coseismic shear heating. *Geophys Res Lett* 34:L14311. <https://doi.org/10.1029/2007GL030049>
- Hirose F, Maeda K (2013) Simulation of recurring earthquakes along the Nankai trough and their relationship to the Tokai long-term slow slip events taking into account the effect of locally elevated pore pressure and subducting ridges. *J Geophys Res* 118:4127–4144. <https://doi.org/10.1002/jgrb.50287>
- Hirose F, Nakajima J, Hasegawa A (2008) Three-dimensional seismic velocity structure and configuration of the Philippine Sea slab in southwestern Japan estimated by double-difference tomography. *J Geophys Res* 113:B09315. <https://doi.org/10.1029/2007JB005274>
- Hori T (2006) Mechanisms of separation of rupture area and variation in time interval and size of great earthquakes along the Nankai Trough, southwest Japan. *J Earth Simul* 5:8–19
- Hori T, Kato N, Hirahara K, Baba T, Kaneda Y (2004) A numerical simulation of earthquake cycles along the Nankai Trough in southwest Japan: lateral variation in frictional property due to the slab geometry controls the nucleation position. *Earth Planet Sci Lett* 228:215–226. <https://doi.org/10.1016/j.epsl.2004.09.033>
- Hori T, Miyazaki S, Mitsui N (2009) A model of earthquake-generation cycle with scale-dependent frictional property: preliminary results and research plan for a project of evaluation for coming Tokai, Tonankai, and Nankai earthquakes. *J Disaster Res* 4:111–117. <https://doi.org/10.20965/jdr.2009.p0111>
- Hori T, Hyodo M, Miyazaki S (2012) Generation mechanism of giant earthquakes in subduction zones with smaller-size interplate earthquakes during interseismic period. In: *Earthquake research and analysis - Seismology, seismotectonic and earthquake geology*. <https://doi.org/10.5772/29249>
- Hyndman RD, Wang K, Yamano M (1995) Thermal constraints on the seismogenic portion of the southwestern Japan subduction thrust. *J Geophys Res* 100:15373–15392. <https://doi.org/10.1029/95JB00153>
- Hyodo M, Hori T, Kaneda Y (2016) A possible scenario for earlier occurrence of the next Nankai earthquake due to triggering by an earthquake at Hyuga-nada, off southwest Japan. *Earth Planets Space* 68. <https://doi.org/10.1186/s40623-016-0384-6>
- Hyodo M, Hori T (2013) Re-examination of possible great interplate earthquake scenarios in the Nankai Trough, southwest Japan, based on recent findings and numerical simulations. *Tectonophysics* 600:175–186. <https://doi.org/10.1016/j.tecto.2013.02.038>
- Imai K, Nishiyama A, Maeda T, Ishibe T, Satake K, Furumura T (2011) Statistical interpretation of the occurrence time of the 1707 Hōei earthquake by historical documents (in Japanese). *Historical Earthquake* 26:99
- Ishibashi K (1998) Was the earthquake of July 9, 1498 in southwest Japan really the great Nankai earthquake? (in Japanese). Abstract 1998 Japan Earth and Planetary Science Joint Meeting Sf-005:313
- Ishibashi K (2004) Status of historical seismology in Japan. *Ann Geophys* 47:339–368. <https://doi.org/10.4401/ag-3305>
- Japan Meteorological Agency (2017) The seismological bulletin of Japan (in Japanese). http://www.data.jma.go.jp/svd/eqev/data/bulletin/index_e.html, (2021-09-01)
- Kanamori H (1977) The energy release in great earthquakes. *J Geophys Res* 82:2981–2987. <https://doi.org/10.1029/JB082i020p02981>
- Kaneda Y, Kawaguchi K, Araki E, Matsumoto H, Nakamura T, Kamiya S, et al. (2015) Development and application of an advanced ocean floor network system for megathrust earthquakes and tsunamis. In: Favali P et al. editors, *Seafloor observatories*. Springer Praxis Books, pp. 643–662. https://doi.org/10.1007/978-3-642-11374-1_25
- Kaneko Y, Avouac J-P, Lapusta N (2010) Towards inferring earthquake patterns from geodetic observations of interseismic coupling. *Nat Geosci* 3:363–369. <https://doi.org/10.1038/NGEO843>
- Kato N (2003) Repeating slip events at a circular asperity: numerical simulation with a rate- and state-dependent friction law. *Bull Earthq Res Inst* 78:151–166
- Kato N, Tullis TE (2001) A composite rate- and state-dependent law for rock friction. *Geophys Res Lett* 28:1103–1106. <https://doi.org/10.1029/2000GL012060>
- Kawaguchi K, Kaneko S, Nishida T, Komine T (2015) Construction of the DONET real-time seafloor observatory for earthquakes and tsunami monitoring. In: Favali P et al. editors, *Seafloor Observatories*. Springer Praxis Books, pp. 211–228. https://doi.org/10.1007/978-3-642-11374-1_10
- Kimura H, Tadokoro K, Ito T (2019) Interplate coupling distribution along the Nankai Trough in southwest Japan estimated from the block motion model based on onshore GNSS and seafloor GNSS/A observations. *J Geophys Res* 124:6140–6164. <https://doi.org/10.1029/2018JB016159>
- Kobayashi A (2014) A long-term slow slip event from 1996 to 1997 in the Kii Channel, Japan. *Earth Planets Space* 66. <https://doi.org/10.1186/1880-5981-66-9>
- Kobayashi A (2017) Objective detection of long-term slow slip events along the Nankai Trough using GNSS data (1996–2016). *Earth Planets Space* 69. <https://doi.org/10.1186/s40623-017-0755-7>

- Kobayashi A, Yamamoto T (2011) Repetitive long-term slow slip events beneath the Bungo Channel, southwestern Japan, identified from leveling and sea level data from 1979 to 2008. *J Geophys Res* 116:B04406. <https://doi.org/10.1029/2010JB007822>
- Kobayashi A, Hirose F, Horikawa H, Hirata K, Nakanishi I (2018) A historical record on the 1707 Hoei Earthquake and Hoei Eruption of Mt. Fuji: Investigation and reprint of the "Memorandum of a large earthquake and an eruption of Mt. Fuji" in the documents of Iisaku Family (in Japanese). *J Seism Soc Jpn* 70:221–231. <https://doi.org/10.4294/zisin.2017-6>
- Kodaira S, Takahashi N, Nakanishi A, Miura S, Kaneda Y (2000) Subducted seamount imaged in the rupture zone of the 1946 Nankaido earthquake. *Science* 289:104–106. <https://doi.org/10.1126/science.289.5476.104>
- Kodaira S, Iidake T, Kato A, Park J, Iwasaki T, Kaneda Y (2004) High pore fluid pressure may cause silent slip in the Nankai Trough. *Science* 304:1295–1298. <https://doi.org/10.1126/science.1096535>
- Kodaira S, Hori T, Ito A, Miura S, Fujie G, Park J-O et al (2006) A cause of rupture segmentation and synchronization in the Nankai trough revealed by seismic imaging and numerical simulation. *J Geophys Res* 111:B09301. <https://doi.org/10.1029/2005JB004030>
- Kuroki H, Ito HM, Yoshida A (2002) A three-dimensional simulation of crustal deformation accompanied by subduction in the Tokai region, central Japan. *Phys Earth Planet Interiors* 132:39–58. [https://doi.org/10.1016/S0031-9201\(02\)00043-2](https://doi.org/10.1016/S0031-9201(02)00043-2)
- Kuroki H, Ito HM, Yoshida A (2004) Effects of nearby large earthquakes on the occurrence time of the Tokai earthquake—an estimation based on a 3-D simulation of plate subduction. *Earth Planets Space* 56:169–178. <https://doi.org/10.1186/BF03353401>
- Lapusta N, Liu Y (2009) Three-dimensional boundary integral modeling of spontaneous earthquake sequences and aseismic slip. *J Geophys Res* 114:B09303. <https://doi.org/10.1029/2008JB005934>
- Lapusta N, Rice JR, Ben-Zion Y, Zheng G (2000) Elastodynamic analysis for slow tectonic loading with spontaneous rupture episodes on faults with rate- and state-dependent friction. *J Geophys Res* 105:23765–23789. <https://doi.org/10.1029/2000JB900250>
- Linker MF, Dieterich JH (1992) Effects of variable normal stress on rock friction: observations and constitutive equations. *J Geophys Res* 97:4923–4940. <https://doi.org/10.1029/92JB00017>
- Liu Y, Rice JR (2005) Aseismic slip transients emerge spontaneously in three-dimensional rate and state modeling of subduction earthquake sequences. *J Geophys Res* 110:B08307. <https://doi.org/10.1029/2004JB003424>
- Maemoku H (1988) Holocene crustal movement in Muroto peninsula, southwestern Japan (in Japanese with English abstract). *Geograph Rev Jpn* 61:747–769. https://doi.org/10.4157/grj1984a.61.10_747
- Matsu'ura R (2012) 1707 Hoei earthquake (on 28 October Hoei 4) (in Japanese). In: Kitahara I, Matsu'ura R, Kimura R, Yoshikawa-koubunkan, editors. *Japanese Historical Disaster Encyclopedia*. pp. 217–222
- Matsubara M, Shiomi K, Baba H, Sato H, Nishimiya T (2021) Improved geometry of the subducting Philippine Sea plate beneath the Suruga Trough. *Global Planet Change* 204:103562. <https://doi.org/10.1016/j.gloplacha.2021.103562>
- Mitsui N, Hirahara K (2006) Slow slip events controlled by the slab dip and its lateral change along a trench. *Earth Planet Sci Lett* 245:344–358. <https://doi.org/10.1016/j.epsl.2006.03.001>
- Mochizuki K, Fujie G, Sato T, Kasahara J, Hino R, Shinohara M, Suyehiro K (1998) Heterogeneous crustal structure across a seismic block boundary along the Nankai Trough. *Geophys Res Lett* 25:2301–2304. <https://doi.org/10.1029/98GL51867>
- Mochizuki K, Yamada T, Shinohara M, Yamanaka Y, Kanazawa T (2008) Weak interplate coupling by seamounts and repeating M–7 earthquakes. *Science* 321:1194–1197. <https://doi.org/10.1126/science.1160250>
- Morishige M, van Keken PE (2017) Along-arc variation in short-term slow slip events caused by 3-D fluid migration in subduction zones. *J Geophys Res* 122:1434–1448. <https://doi.org/10.1002/2016JB013091>
- Mura T (1987) *Micromechanics of defects in solids*. Martinus Nijhoff Publishers, Dordrecht, The Netherlands, 2nd edn, pp. 587.
- Murotani S, Shimazaki K, Koketsu K (2015) Rupture process of the 1946 Nankai earthquake estimated using seismic waveforms and geodetic data. *J Geophys Res* 120:5677–5692. <https://doi.org/10.1002/2014JB011676>
- Nakata R, Hyodo M, Hori T (2014) Possible slip history scenarios for the Hyuganada region and Bungo Channel and their relationship with Nankai earthquakes in southwest Japan based on numerical simulations. *J Geophys Res* 119:4787–4801. <https://doi.org/10.1002/2014JB010942>
- Nakata R, Hori T, Hyodo M, Ariyoshi K (2016) Possible scenarios for occurrence of M–7 interplate earthquake prior to and following the 2011 Tohoku-Oki earthquake based on numerical simulation. *Sci Rep* 6:25704. <https://doi.org/10.1038/srep25704>
- Nakatani M (2001) Conceptual and physical clarification of rate and state friction: frictional sliding as a thermally activated rheology. *J Geophys Res* 106:13347–13380. <https://doi.org/10.1029/2000JB900453>
- Nishimura T, Matsuzawa T, Obara K (2013) Detection of short-term slow slip events along the Nankai Trough, southwest Japan, using GNSS data. *J Geophys Res* 118:3112–3125. <https://doi.org/10.1002/jgrb.50222>
- Nishimura T, Yokota Y, Tadokoro K, Ochi T (2018) Strain partitioning and interplate coupling along the northern margin of the Philippine Sea plate, estimated from GNSS and GPS-A data. *Geosphere* 14. <https://doi.org/10.1130/GES01529.1>
- Noda A, Saito T, Fukuyama E (2018) Slip-deficit rate distribution along the Nankai trough, southwest Japan, with elastic lithosphere and viscoelastic asthenosphere. *J Geophys Res* 123:8125–8142. <https://doi.org/10.1029/2018JB015515>
- Obara K, Kato A (2016) Connecting slow earthquakes to huge earthquakes. *Science* 353:253–257. <https://doi.org/10.1126/science.aaf1512>
- Ochi T (2015) Temporal change in plate coupling and long-term slow slip events in southwestern Japan. *Earth Planet Sci Lett* 431:8–14. <https://doi.org/10.1016/j.epsl.2015.09.012>
- Ochi T, Kato T (2013) Depth extent of the long-term slow slip event in the Tokai district, central Japan: a new insight. *J Geophys Res* 118:4847–4860. <https://doi.org/10.1002/jgrb.50355>
- Ohtani M, Hirahara K (2015) Effect of the Earth's surface topography on the quasi-dynamic earthquake cycles. *Geophys J Int* 203:384–398. <https://doi.org/10.1093/gji/ggv187>
- Okamoto AS, Niemeijer AR, Spier CJ, Takeshita T (2016) Frictional properties of mafic metamorphic gouges: implication for slow earthquakes along the Nankai Trough. *JpGU meeting*, SSS27-19
- Okamura Y, Shishikura M (2020) New hypothesis to explain Quaternary forearc deformation and the variety of plate boundary earthquakes along the Suruga-Nankai Trough by oblique subduction of undulations on the Philippine Sea Plate. *Earth Planets Space* 72(55). <https://doi.org/10.1186/s40623-020-01183-5>
- Okamura M, Matsuoka H (2012) Nankai earthquake recurrences from tsunami sediment (in Japanese). *Kagaku* 82:182–191
- Ozawa S (2017) Long-term slow slip events along the Nankai trough subduction zone after the 2011 Tohoku earthquake in Japan. *Earth Planets Space* 69(56). <https://doi.org/10.1186/s40623-017-0640-4>
- Ozawa S, Tobita M, Yari H (2016) A possible restart of an interplate slow slip adjacent to the Tokai seismic gap in Japan. *Earth Planets Space* 68(54). <https://doi.org/10.1186/s40623-016-0430-4>
- Park J-O, Moore GF, Tsuru T, Kodaira S, Kaneda Y (2003) A subducted oceanic ridge influencing the Nankai megathrust earthquake rupture. *Earth Planet Sci Lett* 217:77–84. [https://doi.org/10.1016/S0012-821X\(03\)00553-3](https://doi.org/10.1016/S0012-821X(03)00553-3)
- Pollitz FF, Sacks IS (1995) Consequences of stress changes following the 1891 Nobi Earthquake, Japan. *Bull Seism Soc Am* 85:796–807
- Press WH, Teukolsky SA, Vetterling WT, Flannery BP (1992) *Numerical recipes in fortran*, 2nd edn. Cambridge Univ. Press, Cambridge, England, p 963
- Radiguet M, Perfettini H, Cotte N, Gualandi A, Valette B, Kostoglodov V et al (2016) Triggering of the 2014 M_w 7.3 Papanoa earthquake by a slow slip event in Guerrero, Mexico. *Nature Geo* 9:829. <https://doi.org/10.1038/NNGEO2817>
- Rice JR (1992) Fault stress states, pore pressure distributions, and the weakness of the San Andreas Fault. In: Evans B, Wong T-F, editors. *Fault mechanics and transport properties of rocks*. Academic Press, pp. 475–503. [https://doi.org/10.1016/S0074-6142\(08\)62835-1](https://doi.org/10.1016/S0074-6142(08)62835-1)
- Rice JR (1993) Spatio-temporal complexity of slip on a fault. *J Geophys Res* 98:9885–9907. <https://doi.org/10.1029/93JB00191>
- Rice JR (2006) Heating and weakening of faults during earthquake slip. *J Geophys Res* 111:B05311. <https://doi.org/10.1029/2005JB004006>
- Rubin AM, Ampuero JP (2005) Earthquake nucleation on (aging) rate and state faults. *J Geophys Res* 110:B11312. <https://doi.org/10.1029/2005JB003686>
- Ruina A (1983) Slip instability and state variable friction laws. *J Geophys Res* 88:10359–10370. <https://doi.org/10.1029/JB088iB12p10359>

- Sakaguchi A, Chester F, Curewitz D, Fabbri O, Goldsby D, Kimura G et al (2011) Seismic slip propagation to the updip end of plate boundary subduction interface faults: vitrinite reflectance geothermometry on Integrated Ocean Drilling Program NanTro SEIZE cores. *Geology* 39:395–398. <https://doi.org/10.1130/G31642.1>
- Sawai M, Niemeijer AR, Plümpner O, Hirose T, Spiers CJ (2016) Nucleation of frictional instability caused by fluid pressurization in subducted blueschist. *Geophys Res Lett* 43:2543–2551. <https://doi.org/10.1002/2015GL067569>
- Scholz CH, Small C (1997) The effect of seamount subduction on seismic coupling. *Geology* 25:487–490. [https://doi.org/10.1130/0091-7613\(1997\)025%3c0487:TEOSSO%3e2.3.CO;2](https://doi.org/10.1130/0091-7613(1997)025%3c0487:TEOSSO%3e2.3.CO;2)
- Seno T (2009) Determination of the pore fluid pressure ratio at seismogenic megathrusts in subduction zones: implications for strength of asperities and Andean-type mountain building. *J Geophys Res* 114:B05405. <https://doi.org/10.1029/2008JB005889>
- Seno T (2012) Great earthquakes along the Nankai Trough: a new idea for their rupture mode and time series (in Japanese with English abstract). *J Seism Soc Jpn* 2(64):97–116. <https://doi.org/10.4294/zisin.64.97>
- Shibazaki B, Matsuzawa T, Tsutsumi A, Ujije K, Hasegawa A, Ito A (2011) 3D modeling of the cycle of a great Tohoku-oki earthquake, considering frictional behavior at low to high slip velocities. *Geophys Res Lett* 38:L21305. <https://doi.org/10.1029/2011GL049308>
- Shibazaki B, Wallace LM, Kaneko Y, Hamling I, Ito Y, Matsuzawa T (2019) Three-dimensional modeling of spontaneous and triggered slow-slip events at the Hikurangi subduction zone, New Zealand. *J Geophys Res* 124:13250–13268. <https://doi.org/10.1029/2019JB018190>
- Shimazaki K, Nakata T (1980) Time-predictable recurrence model for large earthquakes. *Geophys Res Lett* 7:279–282. <https://doi.org/10.1029/GL007i004p00279>
- Shishikura M, Echigo T, Maemoku H, Ishiyama T (2008) Height and ages of uplifted sessile assemblage distributed along the southern coast of the Kii Peninsula, south-central Japan: Reconstruction of multi-segment earthquake history along the Nankai Trough (in Japanese with English abstract). *Annu Rep Active Fault Paleoearthq Res* 8:267–280
- Stuart WD (1988) Forecast model for great earthquakes at the Nankai trough subduction zone. *Pure Appl Geophys* 126:619–641. <https://doi.org/10.1007/BF00879012>
- Suenaga N, Yoshioka S, Matsumoto T (2016) Relationships among temperature, dehydration of the subducting Philippine Sea plate, and the occurrence of a megathrust earthquake, low-frequency earthquake, and a slow slip event in the Tokai district, central Japan. *Phys Earth Planet Inter* 260:44–52. <https://doi.org/10.1016/j.pepi.2016.09.004>
- Tai S (2006) “Shinchoki” recorded about earthquakes and tsunamis in Shishikui, Tokushima (in Japanese). Harada print publishing co. Ltd., pp. 113
- Takagi R, Obara K, Maeda T (2016) Slow slip event within a gap between tremor and locked zones in the Nankai subduction zone. *Geophys Res Lett* 43:1066–1074. <https://doi.org/10.1002/2015GL066987>
- Takagi R, Uchida N, Obara K (2019) Along-strike variation and migration of long-term slow slip events in the western Nankai subduction zone, Japan. *J Geophys Res* 124:3853–3880. <https://doi.org/10.1029/2018JB016738>
- Takayama H, Maeda K, Hirose F (2008) Effect of the plate boundary configuration on the initiation point of great earthquakes along the Nankai trough (in Japanese). *J Seism Soc Jpn* 2(60):279–284. <https://doi.org/10.4294/zisin.60.279>
- Takemura S, Noda A, Kubota T, Asano Y, Matsuzawa T, Shiomi K (2019) Migrations and clusters of shallow very low frequency earthquakes in the regions surrounding shear stress accumulation peaks along the Nankai Trough. *Geophys Res Lett* 46:11830–11840. <https://doi.org/10.1029/2019GL084666>
- Thomas MY, Lapusta N, Noda H, Avouac J-P (2014) Quasi-dynamic versus fully dynamic simulations of earthquakes and aseismic slip with and without enhanced coseismic weakening. *J Geophys Res* 119:1986–2004. <https://doi.org/10.1002/2013JB010615>
- Tsuru T, Park J-O, Miura S, Kodaira S, Kido Y, Hayashi T (2002) A long-arc structural variation of the plate boundary at the Japan Trench margin: Implication of interplate coupling. *J Geophys Res* 107:2357. <https://doi.org/10.1029/2001JB001664>
- Ueno H, Hatakeyama S, Aketagawa T, Funasaki T, Hamada N (2002) Improvement of hypocenter determination procedures in the Japan Meteorological Agency (in Japanese with English abstract). *Quart J Seism* 65:123–134
- Usami T (2003) Materials for comprehensive list of destructive earthquakes in Japan, [416]-2001 [Latest edition] (in Japanese). Univ Tokyo Press, pp. 605
- Utsu T (1961) A statistical study on the occurrence of aftershocks. *Geophys Mag* 30:521–601
- Utsu T (1982) Catalog of large earthquakes in the region of Japan from 1885 through 1980 (in Japanese with English abstract). *Bull Earthq Res Inst* 57:401–463
- Watanabe S, Bock Y, Melgar D, Tadokoro K (2018) Tsunami scenarios based on interseismic models along the Nankai trough, Japan, from seafloor and onshore geodesy. *J Geophys Res* 123:2448–2461. <https://doi.org/10.1002/2017JB014799>
- Wessel P, Smith WHF, Scharroo R, Luis J, Wobbe F (2013) Generic mapping tools: improved version released. *Eos, trans. AGU* 94:409–410. <https://doi.org/10.1002/2013EO450001>
- Working Group to Investigate Disaster Prevention Based on Monitoring and Assessment of Seismicity along the Nankai Trough (2017) Guidance for disaster prevention based on monitoring and assessment of seismicity along the Nankai trough (report) (in Japanese). http://www.bousai.go.jp/jishin/nankai/taio_wg/pdf/h290926honbun.pdf, (2021-09-01)
- Yagi Y, Kikuchi M, Yoshida S, Yamanaka Y (1998) Source process of the Hyuganada Earthquake of April 1, 1968 (MJMA 7.5), and its relationship to the subsequent seismicity (in Japanese with English abstract). *J Seism Soc Jpn* 2(51):139–148. https://doi.org/10.4294/zisin1948.51.1_139
- Yamamoto Y, Obana K, Takahashi T, Nakanishi A, Kodaira S, Kaneda Y (2013) Imaging of the subducted Kyushu-Palau Ridge in the Hyuga-nada region, western Nankai Trough subduction zone. *Tectonophysics* 589:90–102. <https://doi.org/10.1016/j.tecto.2012.12.028>
- Yamashita Y, Shimizu H, Goto K (2012) Small repeating earthquake activity, interplate quasi-static slip, and interplate coupling in the Hyuga-nada, southwestern Japan subduction zone. *Geophys Res Lett* 39:L08304. <https://doi.org/10.1029/2012GL051476>
- Yang H, Liu Y, Lin J (2012) Effects of subducted seamounts on megathrust earthquake nucleation and rupture propagation. *Geophys Res Lett* 39:L24302. <https://doi.org/10.1029/2012GL053892>
- Yokota Y, Ishikawa T, Sato M, Watanabe S, Saito H, Ujihara N, Matsumoto Y, Toyama S, Fujita M, Yabuki T, Mochizuki M, Asada A (2015) Heterogeneous interplate coupling along the Nankai Trough, Japan, detected by GPS-acoustic seafloor geodetic observation. *Prog Earth Planet Sci* 2:10. <https://doi.org/10.1186/s40645-015-0040-y>
- Yokota Y, Ishikawa T, Watanabe S, Tashiro T, Asada A (2016) Seafloor geodetic constraints on interplate coupling of the Nankai Trough megathrust zone. *Nature* 534:374–377. <https://doi.org/10.1038/nature17632>
- Yokota Y, Ishikawa T (2020) Shallow slow slip events along the Nankai Trough detected by GNSS-A. *Sci Adv* 6. <https://doi.org/10.1126/sciadv.aay5786>

Publisher's Note

Springer Nature remains neutral with regard to jurisdictional claims in published maps and institutional affiliations.

Submit your manuscript to a SpringerOpen® journal and benefit from:

- Convenient online submission
- Rigorous peer review
- Open access: articles freely available online
- High visibility within the field
- Retaining the copyright to your article

Submit your next manuscript at ► [springeropen.com](https://www.springeropen.com)